Haze in Pluto's atmosphere: Results from SOFIA and ground-based observations of the 2015 June 29 Pluto occultation

Michael J. Person[a], Amanda S. Bosh[a,b], Carlos A. Zuluaga[a], Amanda A. Sickafoose[c,a], Stephen E. Levine[b,a], Jay M. Pasachoff [d,y], Bryce A. Babcock[d], Edward W. Dunham[b], Ian S. McLean[e], Jürgen Wolf [f,l], Fumio Abe[g], E. E. Becklin[h,e], Thomas A. Bida[b], Len P. Bright[b], Tim Brothers[a], Grant Christie[i], Rebecca F. Durst[d], Alan C. Gilmore[j], Ryan T. Hamilton[b], Hugh C. Harris[k], Chris Johnson[e], Pamela M. Kilmartin[j], Molly Kosiarek[a], Karina Leppik[h], Sarah E. Logsdon[z], Robert Lucas[m], Shevill Mathers[n], C. J. K. Morley[o], Peter Nelson[p], Haydn Ngan[i], Enrico Pfüller[f,l], Tim Natusch[i], Stephanie Sallum[r], Maureen L. Savage[h], Christina H. Seeger[d], Ho Chit Siu[a], Chris Stockdale[s], Daisuke Suzuki[t], Thanawuth Thanathibodee[u], Trudy Tilleman[k], Paul J. Tristram[v], William D. Vacca[h], Jeffrey Van Cleve[h], Carolle Varughese[w], Luke W. Weisenbach[u], Elizabeth Widen[x], Manuel Wiedemann[f,l]

[a]MIT, Department of Earth, Atmospheric, and Planetary Sciences, 77 Mass. Ave., Cambridge, MA 02139
mjperson@mit.edu

[b]Lowell Observatory, 1400 W. Mars Hill Rd., Flagstaff, AZ 86001

[c]South African Astronomical Observatory, P.O. Box 9, Observatory, 7935, Cape Town, South Africa

[d]Williams College, Astronomy Department, 33 Lab Campus Drive, Williamstown, MA 01267

[e]UCLA
Department of Physics and Astronomy, 430 Portola Plaza, Los Angeles, CA 90095-1547

[f]Deutsches SOFIA Institut, Universität Stuttgart, Pfaffenwaldring 29, D-70569 Stuttgart, Germany

[g]Institute for Space-Earth Environmental Research, Nagoya University, Nagoya 464-8601, Japan

[h]SOFIA-USRA
NASA Ames Research Center, Mail Stop N232-12, Moffet Field, CA 94035-1000

[i]Auckland Observatory
670 Manukau Rd, Epsom, Auckland 1345, New Zealand

[j]Department of Physics and Astronomy, University of Canterbury, Christchurch 8041, New Zealand

[k]U.S. Naval Observatory, 10391 W. Naval Obs. Rd., Flagstaff AZ 86001

[l]SOFIA
SOFIA Science Center, NASA Ames Research Center, MS211-1, Moffett Field, CA 94035, USA

[m]Sydney, Australia

[n]Southern Cross Observatory, 819A Cambridge Road Cambridge Tasmania 7170 Australia

[o]Sandy Ridge Observatory, PO Box 459, Moe, Victoria 3825, Australia

[p]Ellinbank Observatory
Victoria, Australia

[r]University of Arizona
Astronomy Department, 933 North Cherry Ave., Tucson, AZ 85721

[s]Hazelwood Observatory
Churchill, Victoria, Australia

[t]Dept. of Physics, University of Notre Dame, Notre Dame, IN 46556, USA

[u]MIT, Department of Physics, 77 Mass. Ave., Cambridge, MA 02139

[v]Mt. John Observatory, P.O. Box 56, Lake Tekapo 7945, New Zealand

[w]State Highway 8, Lake Tekapo 7945, Earth & Sky Limited

[x]United States Antarctic Program, McMurdo Station, Antarctica

[y]Planetary Sciences Department, California Institute of Technology 150-21, 1200 E. California Blvd., Pasadena, CA 91125

[z]NASA Goddard Space Flight Center, Greenbelt, MD 20771

Keywords:
Pluto, atmosphere
Atmospheres, structure
Occultations

1 Abstract

On UT 29 June 2015, the occultation by Pluto of a bright star (r'=11.9) was observed from the Stratospheric Observatory for Infrared Astronomy (SOFIA) and several ground-based stations in New Zealand and Australia. Pre-event astrometry allowed for an in-flight update to the SOFIA team with the result that SOFIA was deep within the central flash zone (~22 km from center). Analysis of the combined data leads to the result that Pluto's middle atmosphere is essentially unchanged from 2011 and 2013 (Person et al. 2013; Bosh et al. 2015); there has been no significant expansion or contraction of the atmosphere. Additionally, our multi-wavelength observations allow us to conclude that a haze component in the atmosphere is required to reproduce the light curves obtained. This haze scenario has implications for understanding the photochemistry of Pluto's atmosphere.

2 Introduction

Pluto possesses a tenuous atmosphere composed of N_2, CO, CH_4, and other trace gases. Close to the icy surface, this atmosphere is in vapor-pressure equilibrium with the ices that exist on the surface. Rising above the surface, the presence of methane in the atmosphere acts as a thermostat to regulate the temperature at approximately 100 K (Yelle and Lunine 1989; Strobel et al. 1996; Zalucha et al. 2011). This atmosphere is loosely bound to Pluto, with its upper reaches being stripped away by the solar wind (Bagenal et al. 2015; McNutt et al. 2015). With continuous resupply by the surface ices, this can lead to a 0.5 - 3 km loss of ice thickness over 4.5 Gyr.

Stellar occultations provide a method for measuring the temperature and pressure of a planetary atmosphere from the Earth. The occultation star P20150629 (UCAC2 139-209445), at r' = 11.941, is one of the two brightest occultation stars for Pluto ever observed (Table 1). An occultation by the brightest star to date was observed in 2010 from only a few stations and while low in the sky (Young et al. 2010).

The resolution limit of stellar occultations, ~2 km at Pluto at visible wavelengths, allows for multiple sample points per 60-km scale height in the atmosphere. During a stellar occultation, flux from the star decreases due to refraction by the planetary atmosphere. The rate of decrease is a function of the temperature and mean molecular weight. By assuming a mainly N_2 atmosphere (Lellouch et al. 2009), we thus determine the temperature as a function of height .

Pluto's atmospheric structure is a topic of special concern as a decrease in solar insolation is predicted to lead to a decrease in atmospheric pressure (Young 2013) or a complete collapse (Hansen et al. 2015). While some earlier models predicted that collapse would already be underway (Hansen and Paige 1996), observations have shown this not to be the case (Bosh et al. 2015a; Dias-Oliveira et al. 2015; Person et al. 2013; Olkin et al. 2015). A delay in this collapse or decrease may be due to such factors as thermal

emissivity of the surface components; thus, the timing of the onset of atmospheric change is a marker of surface-atmosphere interactions.

Table 1. Event parameters

	P20150629
Geocentric midtime (UT)	2015 June 29 16:55:35 ± 00:00:18
Earth ephemeris	DE405
Pluto ephemeris	PLU017
Catalog position equinox and epoch	(J2000; epoch of event)
Catalog & ID	UCAC2 139-209445
R.A.[1] Dec.[1] $\mu_\alpha \cos \delta$ (mas/yr)[2] μ_δ (mas/yr)[2]	19 00 49.4887 ± 0.1370 –20 41 40.896 ± 0.1280 –2.5 ± 1.9 +5.2 ± 1.8
Measured position equinox and epoch	(J2000; epoch 2015.5)
R.A.[§] Dec.[§]	19 00 49.4736 ± 0.0133 –20 41 40.825 ± 0.013
Geocentric close approach (arcsec)	0.169 ± 0.024
Geocentric sky-plane velocity (km/sec)	23.84
Magnitudes[3]	
Filter/Central Wavelength	
B 450nm	12.793 ± 0.046
V 550nm	12.100 ± 0.022
g' 475nm	12.449 ± 0.006
r' 625nm	11.941 ± 0.025
i' 750nm	11.741 ± 0.034
J 1250nm	10.904 ± 0.02
H 1650nm	10.641 ± 0.02
K 2200nm	10.554 ± 0.02

[1]Positions in hms for RA, dms for Dec. Position errors (1 sigma) are in arcseconds.
[2]Angular velocities (proper motions) in milliarcseconds per year from UCAC2 catalog.
[3]BVgri magnitudes are from APASS DR8 (Henden and Munari 2014; Henden et al. 2015). JHK magnitudes are from 2MASS (Skrutskie et al. 2006).

Beyond being one of the brightest events for Pluto, the timing of this event was also important—15 days before the New Horizons spacecraft's close approach to Pluto. Shortly after the close approach, the spacecraft was in a position to observe a pair of occultations by Pluto: (1) an occultation of the Sun observed in the UV with ALICE,

sensitive to Pluto's upper atmosphere at pressures nanobars to microbars and (2) an occultation of a radio signal from Earth, observed with REX, sensitive to Pluto's lower atmosphere at pressures of ~10 microbar. These are above and below the sensitive region for stellar occultations observed from Earth. The P20150629 event occurred within just 2.5 Pluto days of the New Horizons encounter (Bosh et al. 2015b; Sickafoose et al. 2015; Person et al. 2015; Pasachoff et al. 2015), thus it is unlikely that there are any temporal differences. This event, when combined with New Horizons data, produces a complete picture of Pluto's atmosphere at one point in time, which highlights the desirability of continuing to monitor Pluto's atmosphere for the next decade at least.

3 Prediction

Our early predictions, beginning in 2013, placed this event over Australia/New Zealand and its surrounding oceans. We obtained positions for Pluto and the occultation star from 2013 through the night before the event (7 hours before, with observations from the opposite hemisphere), at the four telescopes listed in Table 2. The star positions were averaged via a weighted mean. The Pluto positions were measured, with a center-of-light fitted via a Gaussian point-spread function; Charon's position was explicitly included as a second Gaussian fixed at its ephemeris position. All astrometric field solutions were linear; data from all telescopes were tested prior to this event to assure that this was a valid assumption and that no higher-order terms were needed.

For an occultation such as this, where the observing sites include a mobile station like SOFIA, the expectations on the prediction effort were high. By accurately accounting for all factors in the astrometry, we had the possibility of directing SOFIA to be within Pluto's small central flash zone: previous observations suggest a zone no wider than ±75 km around the geometric center (Olkin et al. 2014).

Pluto's angular diameter is roughly 100 milli-arcseconds. The central-flash region subtends about 5 milli-arcseconds. For stars in our primary astrometric reference catalog (UCAC2), with magnitudes between 10 and 14 in the UCAC2 catalog (Zacharias et al. 2004), typical random astrometric uncertainties at the mean epoch of the observations used to determine the stars' positions are on average 20 mas. These increase to roughly 70 mas by magnitude 16. These uncertainties are lower limits that do not include such things as systematic uncertainties in the star catalogs, and uncertainties in Pluto's position and the difference between its center of light (COL) and center of mass. To predict the location of a 5 mas diameter region required accuracies roughly an order of magnitude better than the then best available astrometric catalog uncertainties. This process is greatly aided today by the release of the GAIA astrometric catalogs (Brown et al. 2018; Perryman 2002).

The astrometry effort took place over the two years prior to the event. Positions for Pluto and the occultation star were updated. We model the observed offset of Pluto from its ephemeris using our Ephemeris Correction Model (ECM); the ECM, a first-order periodic fit to the offsets of the JPL ephemerides based upon our history of astrometric measurements, is useful for early prediction estimates. By the time Pluto and the star are

within the same imager field, we abandon the ECM and perform relative astrometry directly between them. As displayed in Fig. 1, we consider many other effects beyond the positions of Pluto (orange) and the star (red). These additional effects are all of the same scale or larger than the central flash zone; thus failure to account for them may mean missing the central flash. Undetected stellar duplicity (light blue in Fig. 1) is one of the largest additional effects, with the potential to shift the shadow path by 500 mas or more. A close double star would be unresolved in our usual astrometric data, with point spread functions (PSFs) of 0.8 – 1.5 arcsec. An unresolved, equal-magnitude double would produce two shadow paths on the Earth, each 500 mas from the shadow path of the center of light of the two stars. An offset of this magnitude would result in SOFIA missing both shadows and not seeing any occultation. We acquired resolved AO images of the occultation star at Keck with NIRC-2 and Magellan with Mag-AO and Clio (Close et al. 2010) to search for duplicity, both in the K band; we found the star to be single, with a remaining uncertainty of 40 mas for an undetected equal-magnitude companion. This accuracy was sufficient to place SOFIA confidently within the shadow path, but left open the possibility of missing the central flash if the star was still unresolved with a separation between 10 and 40 mas.

Over the year preceding the occultation, Pluto's path among the field stars varied with respect to its ephemeris in an approximately linear fashion. This offset was calculated and extrapolated to the event time. As Pluto neared the star, the error in the extrapolation decreased until approximately one week prior to the event, when Pluto and the star were within the same field; at this time, we switched to relative astrometry. In past events, it was not uncommon for Pluto's calculated position to jump suddenly, by 50-200 mas, presumably due to zonal errors in the UCAC2 catalog or due to compounded proper motion uncertainties, depending on the distribution of high proper-motion stars in the fields (dark blue in Fig. 1). With this event however, there was no such jump and the prediction wavered around New Zealand from our earliest predictions right up through the event.

As we performed astrometry on Pluto, it was important to remember that we were measuring the center of light of the body (yellow bar in Fig. 1). Although Pluto and Charon were blended in our images, we explicitly accounted for Charon in our PSF fits, therefore we measured the center of light of Pluto. For a spherical body with uniform albedo, the center of light would be coincident with the center of mass. For a body with stark albedo contrast (such as Iapetus), the center of light may be offset from the center of mass by as much as half of the body radius. In order to apply this to Pluto, we needed to know its albedo distribution. While albedo maps have been constructed from prior Earth-based observations (Buie et al. 2010), there was a possibility that the albedo distribution had changed due to volatile sublimation or deposition. To account for the current albedo distribution, we took advantage of the low-resolution images coming in from New Horizons. The resolution of the images was sufficient that we could attempt to approximate the center of light offset. To do this, we modelled the changing observed shift in Pluto's position prediction caused by the changing center of light offset throughout Pluto's rotation. The result of this final astrometric shift was to send directions to SOFIA, while it was already airborne during the occultation flight, to fly

330 km north of the previously predicted path. This final shift corresponded to about 12 mas, which was about twice our formal error for the final prediction.

<Insert sideways Figure 1 here>

Table 2. Telescopes used for astrometry in 2015

Name	DCT	L42	NOFS	SARA-CT
Aperture (m)	4.3	1.1	1.55	0.6
Location	Happy Jack, AZ	Anderson Mesa, AZ	Flagstaff, AZ	Cerro Tololo, Chile
Latitude	34° 44' 39.8"	35° 05' 48.3"	35° 11' 02.4"	–30° 10' 19.6"
E. Longitude	–111° 25' 19.9"	–111° 32' 07.9"	–111° 44' 25.9"	–70° 47' 57.0"
Altitude (m)	2360	2206	2273	2126
# nights	6	17	27	21
# frames	304	725	465	3243

4 Data

From our early prediction efforts, we knew that the occultation shadow would pass over New Zealand; as a result, our observational efforts were focused there. In addition to SOFIA, the airborne observatory, we also required observations from several ground stations, to significantly improve the ability to determine the geometry of the event. At the same time as extensive prediction efforts were underway to provide updates to SOFIA, ground-based observers were deployed to cover the expected ground track, with sufficient duplication to allow for locally cloudy weather and other issues that might arise. We summarize the observing circumstances of each of the stations in our group. Other groups were also deployed around New Zealand and Australia (Sicardy et al. 2016) (Young, E. *et al.* in prep.).

4.1 SOFIA

We observed the occultation star on two nights, 28 and 29 June 2015 UT, from the NASA/DLR Stratospheric Observatory for Infrared Astronomy (SOFIA) aircraft (Becklin et al. 2007), during its 2015 Southern Deployment to Christchurch New Zealand. We were able to observe the occultation by Pluto in both the optical and near infrared using three different instruments: the High Speed Imaging Photometer for Occultations (HIPO) (Dunham et al. 2004), the First Light Infrared Test Camera (FLITECAM) (McLean et al. 2006; Logsdon et al. 2014) and the Focal Plane Imager (FPI+)(Wolf et al. 2014).

The first night we did basic instrument calibrations, signal to noise measurements, and filter selection. This also allowed the aircrew to practice maneuvering to place the aircraft at the correct location at a precise time, while on the Pluto observation heading. After analyzing the images from this first night, we decided to use open filters on all visible instruments (both HIPO channels and FPI+), and to use the 1.8-micron blocking filter on FLITECAM to minimize background glare while maximizing overall stellar signal to noise. Taking into account the optics along the light path, the detector quantum

efficiency (QE) and the stellar spectral energy distribution, the effective observation central wavelengths were 0.57 micron (HIPO Blue), 0.65 micron (FPI+), 0.81 micron (HIPO red), and 1.8 micron (FLITECAM).

The second night of observations included a setup flight leg for focusing the telescope and setting initial camera parameters, a Pluto calibration flight leg for verifying signal-to-noise ratio (SNR) estimates, and then a long maneuvering leg to get the aircraft into the correct place to approach the occultation central flash region on the Pluto heading. During this maneuvering leg, the final astrometric prediction update was sent to the aircraft from Lowell Observatory, in Flagstaff, AZ, USA, using both the dedicated SOFIA data link (SkyNet) and a satellite phone. Because of this update, the flight plan was adjusted, moving the aircraft over 300 km north of the route planned at takeoff, and resulting in an intercept location over the south island of New Zealand (Fig. 2).

Once on the Pluto leg, and after a small diversion to correct the intercept timing, all three instruments were set for continuous GPS timed observations of the event. For timing calibration, secondary chopping was done before the occultation between 16:39:00 and 16:41:00 UT and after the event between 17:05:00 and 17:07:00 UT. This provided known simultaneous events in all SOFIA cameras to confirm individual timing systems' simultaneity.

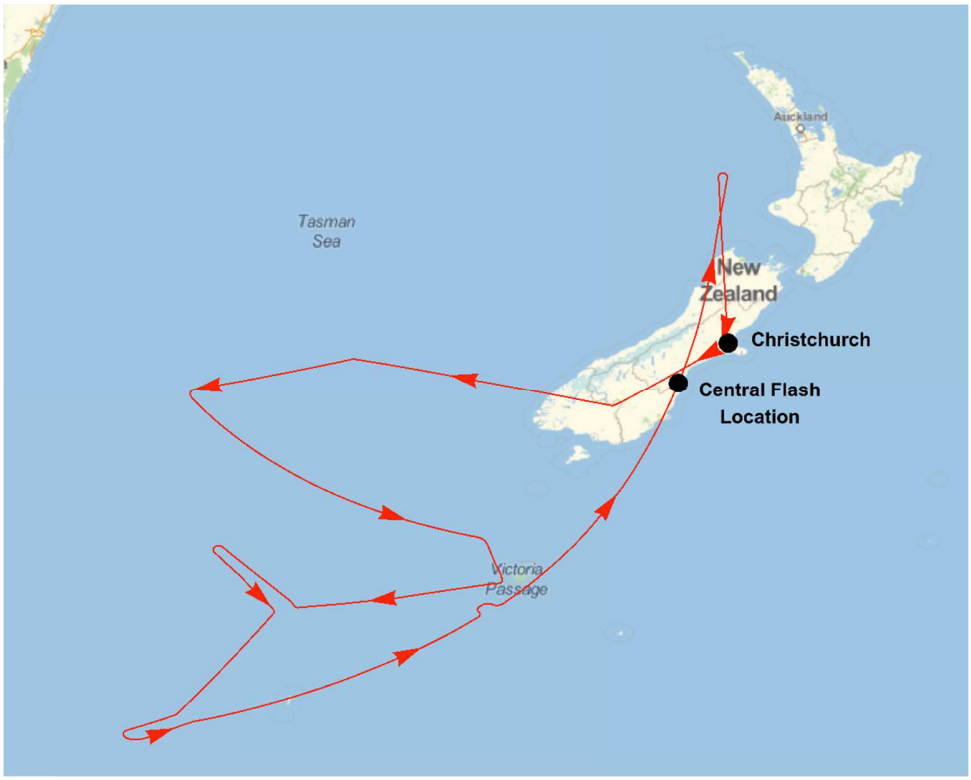

Fig. 2. Path of SOFIA during the stellar occultation flight. Following departure from Christchurch, SOFIA flew to the southwest before returning to New Zealand along the mostly smooth curve. The "wiggle" in the flight path just below the label "Victoria Passage" was inserted in order to ensure that SOFIA arrived at the center of the occultation path (indicated by the black dot) at the predicted midtime of the event.

4.1.1 HIPO

The HIPO cameras—red and blue—both use E2V back-illuminated deep-depletion frame transfer CCDs with millisecond level deadtime between images. The cameras were binned 4x4, giving an effective pixel size of 1.3 arcseconds/pixel. The images were triggered off integrated GPS units every 0.2 seconds. The HIPO red channel occultation run started at 16:38:00 UT, and the HIPO blue channel imaging run started at 16:38:10 UT. Each ran for 30 minutes. The HIPO red and blue data were both reduced using a 7-pixel radius circular aperture. Sky background estimates were taken from nearby blank sky apertures. Two comparison stars in the field were measured in the same manner and used to correct for variability.

4.1.2 FPI+

The FPI+ (Pfueller et al. 2018) uses an Andor iXon EM+ DU-888-#BV camera that has a single back-illuminated, electron-multiplying EM-CCD and was used unfiltered. The images were binned 2x2 for an effective plate scale of 1.0 arcseconds/pixel. The occultation run was started at 16:26:45.6 UT. The integration time was 0.2 seconds and the cycle time was 0.227 seconds. FPI+ images were triggered internally and then time-tagged from the GPS. Images were taken for 42m:21s. The data were reduced using an 8 pixel radius circular aperture with sky background measurements taken from a nearby blank sky region, and as with the HIPO images, two comparison stars were measured as well.

4.1.3 FLITECAM

FLITECAM is a near-infrared imager and grism spectrograph covering the 1 to 5 micron range (McLean *et al*. 2006, Logsdon *et al*. 2014). FLITECAM's 1024x1024 InSb ALADDIN III array covers an 8 arcmin diameter field of view with a plate scale of 0.475 arcsec per pixel. Images were obtained using the FLITECAM H-wide filter, which is centered near 1.8 microns (1.55 to 2.15 microns). This filter is intended for use as an order-sorting filter in FLITECAM's grism spectroscopy mode; however, it was employed for these observations in order to maximize the signal from the source while minimizing the background and simultaneously extending the observations to the longest wavelengths possible. FLITECAM was co-mounted with the HIPO instrument during these observations. The integration time on chip was 1.25 seconds and the dead time was 0.55 seconds per frame, for an effective cycle time of 1.8 seconds. The start times and cycle times were calibrated before the observations relative to HIPO data and the GPS. The data were reduced with an 8-pixel radius circular aperture. Sky background was estimated from surrounding blank sky. Comparison stars were also measured.

4.2 Mt. John Observatory: 1-m, OC 0.61-m, and B&C 0.61-m

Details of data collection from the Mt. John Observatory (MJO) 1-m McLellan Telescope (unfiltered visible), the 0.61-m Optical Craftsmen (OC) Telescope (near-IR: 1.25μ), and the 0.61-m Boller & Chivens (B&C) Telescope (at g', r', and i') are given in Pasachoff *et al*. (2017). We present the observing parameters from these telescopes in Table 3. We also present the light curves from these telescopes in Fig. 3.

4.3 Auckland Observatory (Stardome Observatory): 0.5-m and 0.4-m

Observations were taken on two telescopes at the Auckland Observatory, in Auckland, New Zealand: the 0.5-m Edith Winstone Blackwell Telescope and the 0.4-m Meade ACF telescope. The 0.5-m is a Zeiss on an offset German Equatorial mount with f/13.3 at Cassegrain focus. A Portable Occultation Eclipse and Transit System - POETS (Souza et al. 2006) instrument was mounted on the 0.5-m and had a plate scale of 0.5 arcseconds/pixel. POETS was GPS-triggered, with a cycle time of 0.4 sec (0.0017 second deadtime), in full-frame, 1 MHz readout with the conventional CCD amplifier. These settings returned 5.51 electron/pixel read noise, 1.43 electron/ADU gain, and negligible dark current at -60 C.

The 0.4-m telescope is an f/10 at Cassegrain focus, on which a Portable Instrument for Capturing Occultations - PICO (Lockhart et al. 2010) instrument was mounted. The plate scale was 1.1 arcseconds/pixel and the GPS-triggered cycle time was 2 sec (0.76 seconds deadtime). The PICO data had 13.9 electron/pixel read noise, 1.83 electron/ADU gain, and ~0.3 electrons/pixel/sec of dark current at -40 C.

Data were acquired on both telescopes two nights prior to, as well as a few hours before, the occultation when Pluto and the star were well separated. One-hour occultation data cubes were taken starting at 16:25:00 UT. Weather conditions were highly variable, with interspersed cloud and light rain. The field became visible with seeing ~2.5 arcseconds approximately one minute before immersion and was clouded over before emersion, resulting in partial light curves from both telescopes.

4.4 Other sites

Observations were planned and prepared for at several other sites, including in Tasmania, coastal Victoria near Melbourne, and McMurdo Station in Antarctica. Unfortunately, these observations were not successful due to a variety of reasons including weather, equipment problems, and illness.

4.5 Light curve normalization

All data sets were calibrated in a standard fashion, using biases, flats (when available), and on-chip reference stars. Because the fields of view for the instruments are different (Table 2), the choice of on-chip reference stars varied. The light curves were normalized by the ratio of the occultation star to the combined Pluto plus Charon signal, measured on the night of the occultation roughly four hours prior to the event when they were sufficiently separated. The Pluto-to-star ratio is critical for the calibration of the residual flux at the bottom of each light curve. The fully normalized light curves are shown in Fig. 3; they are plotted against time from the midpoint of each observation. Because the observing stations are distributed in longitude on the Earth, the midtime of each chord differs by a few seconds.

5 Analysis

The set of light curves from SOFIA were all acquired through the same beam, using beamsplitters and dichroics. Each light curve was acquired individually so that integration parameters are different for each. A key characteristic of the set of SOFIA light curves (Fig. 3) is the prominent central flash visible in all (Person et al., in preparation). Positive spikes in the light curve are visible on both ingress and egress as well; these have been associated with small changes in local temperature (Pasachoff et al., 2017). Both ingress and egress show a three-part slope reminiscent of light curves from 2011 and 1988. After occultation onset at full flux, the slope becomes shallower at ~40% flux, followed by a steeper drop at 15% flux. This lower region is partially disguised by the spikes in the light curve and therefore is more difficult to see.

The MJO and Auckland light curves show similar characteristics to the SOFIA data, with some differences. MJO was further from the shadow center, therefore the central flash height is lower but still visible. Auckland was even further from the shadow center and so no central flash is expected from this station. From this site, data could not be collected during the entire event, as thick clouds obscured egress. Data collected stopped just after the event midtime and no central flash was seen, consistent with the geometric solution.

<Insert sideways Table 3 here>

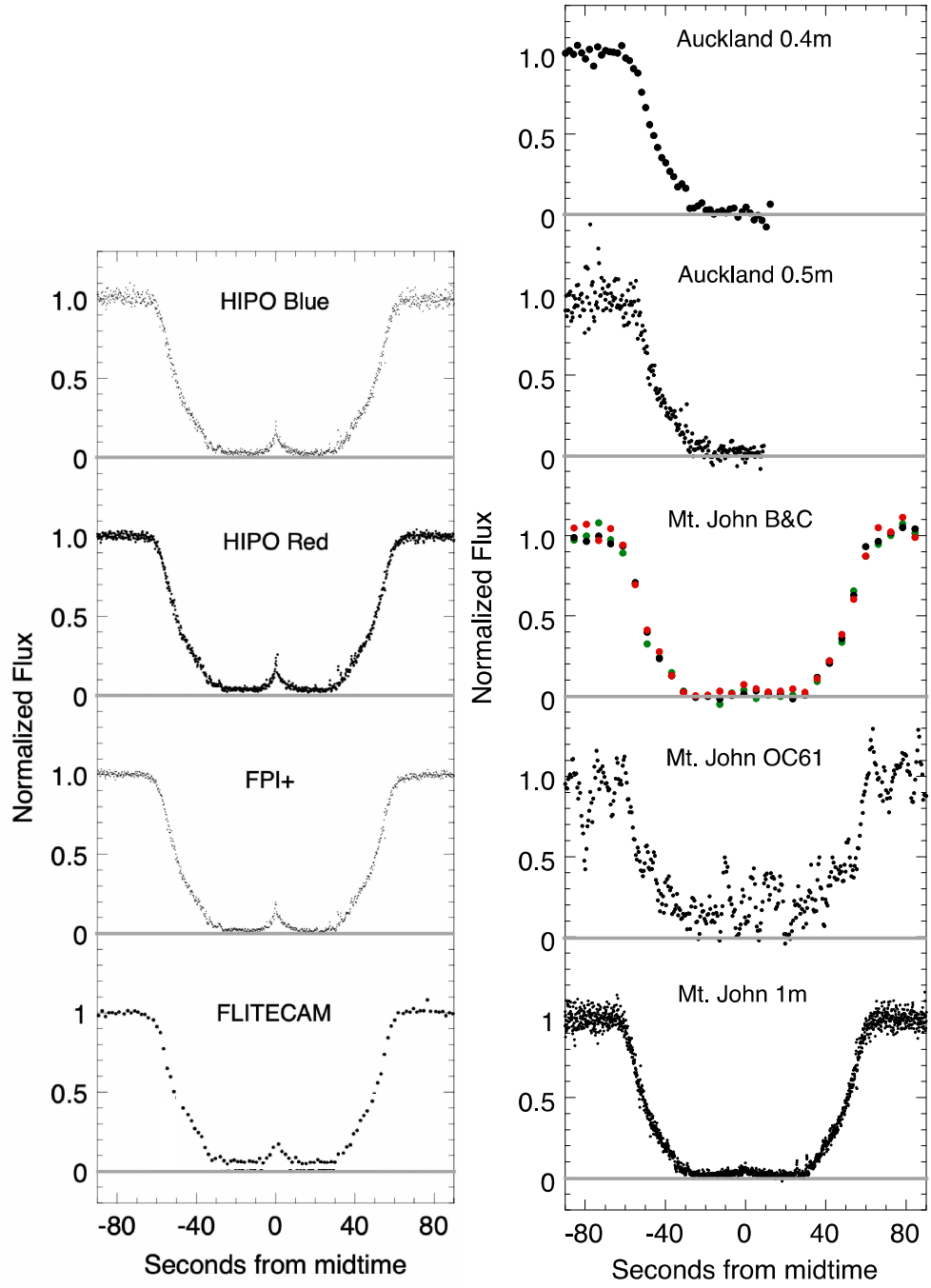

Fig. 3. Light curves from the occultation of P20150629 by Pluto. The left panel shows light curves obtained aboard SOFIA while the right panel shows light curves obtained from ground-based sites, ordered by observed Pluto impact parameter, with more northerly curves at the top and centerline curves at the bottom. The effective central wavelength for each observation is: 0.57 micron for HIPO Blue, 0.81 micron for HIPO Red, 0.65 micron for FPI+, 1.8 micron for FLITECAM, 0.60 micron for the Auckland 0.5-m and the Mt. John 1-m observations, 0.65 micron for the Auckland 0.4-m, 1.25 micron for the Mt. John OC61, and (0.4770, 0.6231, and 0.7625) micron for the Mt. John B&C.

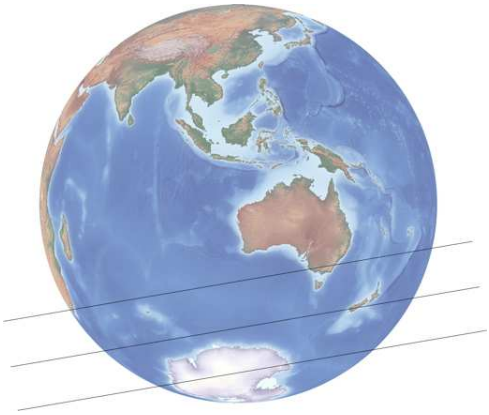

Fig. 4. Geometric solution for Pluto shadow path on Earth.

We begin analysis by calculating the solution for the geometry of the occultation using a subset of light curves; HIPO, FPI+, FLITECAM, MJO-1m, and Auckland-0.5m. While the position difference between the most northerly station (Auckland) and the most southerly station (SOFIA) is only 524 km at midtime, this is sufficient to solve for the event geometry. In addition, the two chords through the central flash act to further constrain the geometry. The model used is that of Elliot & Young (1992) and allows for a constant thermal gradient throughout the atmosphere as well as a haze layer with defined turn-on radius and scale height. We present these results in Table 4, both for clear- and hazy-atmosphere assumption, along with comparison results from 2011 and 2013. The center line offsets for each model are listed in Table 5. The projection of the shadow on the Earth is shown in Fig. 4, and the occultation trajectory across Pluto is shown in Fig. 5.

Table 4. Pluto atmosphere model fits

	PC20110623	P20130504	P20150629	P20150629
	temperature gradient above half light	temperature gradient above half light	temperature gradient above half light (current work)	haze model (current work)
χ^2 per degree of freedom	1.11	1.22	1.11	1.07
Shadow radius (km)	1156 ± 17	1188.7 ± 7.7	1213.83 ± 1.10	1229.2 ± 0.6
H_P (km)	61.2 ± 1.0	54.4 ± 0.5	52.8 ± 0.7	57.3 ± 0.7
P_h (μbar)	2.39 ± 0.12	1.66 ± 0.03	1.37 ± 0.03	1.52 ± 0.04
T_h (K)	110.7 ± 1.7	94.6 ± 1.0	92.4 ± 1.2	100.1 ± 1.3
dT/dr (K/km)	–0.24 ± 0.03	–0.24 ± 0.01	–0.16 ± 0.01	–0.08 ± 0.01
r_h (km)	1273.1 ± 4.0	1299.2 ± 3.8	1295.0 ± 0.5	1296.1 ± 0.5
λ_h	14.0 ± 0.9	15.6 ± 0.3	18.8 ± 0.2	20.0 ± 0.1
b	–2.7 ± 0.4	–3.3 ± 0.2	–2.3 ± 0.2	–1.1 ±0.1
f_0 (km)		–2601.5 ± 1.5	954.3 ± 3.7	952.7 ± 0.4
g_0 (km)		2856 ± 14	1.7 ± 21.8	11.5 ± 0.9

Atmospheric model parameters H_P (half-light pressure scale height), P_h (half-light pressure), T_h (half-light temperature), dT/dr (temperature gradient), r_h (half-light radius), λ_h (thermal energy ratio) and b (thermal gradient exponent) are fully defined in Elliot, Person and Qu, 2003.

Table 5. P20150629 impact parameters

	Close Approach Distance (km)
SOFIA	22.8 S of center
Mt. John	53.1 N of center
Auckland	491.2 N of center
Uncertainty	0.9

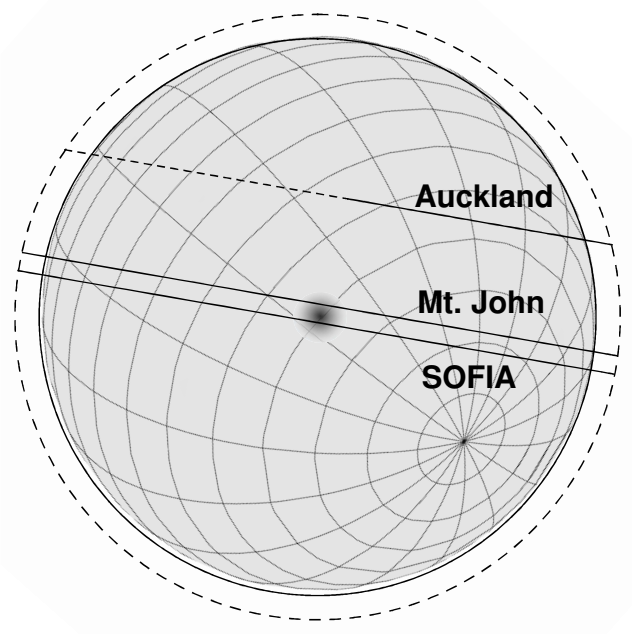

Fig. 5. Approximate path of star as seen on Pluto from the Earth. The SOFIA and Mt. John occultation chords were central, with ingress occurring near the pole and egress occurring near the equator. The outer dashed line represents the half-light level in the atmosphere, or approximately 1300 km from the center of Pluto. The solid chords across Pluto show the observed apparent paths of the star relative to Pluto as from SOFIA, Mt. John, and Auckland observing sites. However, as seen from any of these sites, as the star enters the atmosphere it dims and appears to travel along the limb of Pluto. The Auckland chord is solid for only half of its length because the event egress was clouded out as seen from this site; the cloudy portion is dashed. The spot in the center indicates the location of the central flash, although the extent is exaggerated in order to make the zone visible at this scale.

6 Atmosphere Results

6.1 Models

One representative light curve from SOFIA is shown in Fig. 6. The data points are plotted as open circles. The two models of Table 4 are over-plotted: (i) the model with a clear atmosphere with thermal gradient including data only down to half light is plotted as a heavy dashed line while (ii) a hazy atmosphere with thermal gradient is plotted as a solid line. Both models fit equally well above flux levels of ~30%, a feature noted by Bosh et al. (2015). The upper light curve levels are insensitive to the lower light curve features. Below ~30% flux, the data deviate strongly from a simple, constant thermal gradient model. This is particularly evident in the very strong central flash predicted by the clear atmosphere model but not seen in the data.

In contrast, the haze model with a simple thermal gradient fits well to the entire data set. (Although this could be corrected without invoking haze by instead invoking a stronger thermal gradient below the occultation sampling regions as in Sicardy et al. 2016.) The general character of the "knee" at 30% is reproduced, as is the depressed central flash. The central flash region is sensitive to the near-surface atmosphere (~50km altitude), as well as to atmospheric oblateness. Further analysis of the central flash region will be presented in Person et al. (2019, in prep).

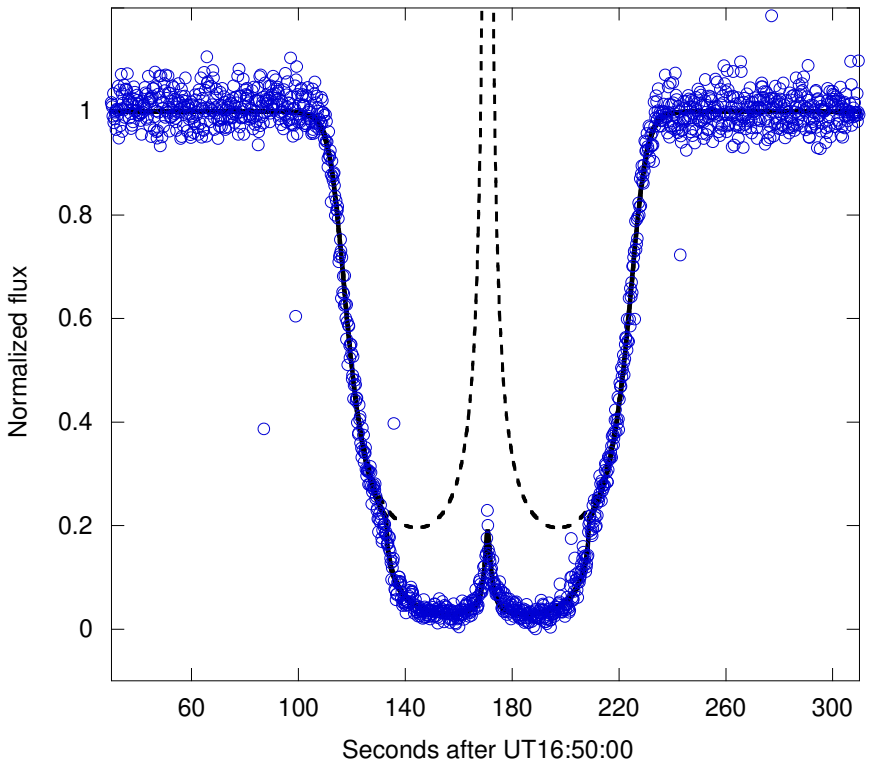

Fig. 6. HIPO-blue data, comparison of haze model and clear-atmosphere model. This full-resolution data plot is representative of the model plots for all datasets. The solid heavy line is the haze model, while the dashed line represents the single-gradient clear atmosphere model. Both models include a thermal gradient. The haze model includes all data in the fit, while the clear atmosphere model includes data only between flux levels of 0.5 and 1.0. A clear atmosphere model fit was attempted using all data, but the parameters quickly became non-physical. Note that the addition of haze in the atmosphere reproduces both the increased slope near the bottom of the curve as well as the height of the depressed central flash level.

6.2 Inversion

While the modeling presented above predicts a light curve from a simple atmospheric model, it is likely that Pluto's atmosphere sports a more complex structure than our model currently incorporates. A stratopause, or temperature maximum, is seen in other atmospheres such as Titan's (Sicardy et al. 2006). At the stratopause, the temperature structure transitions from a positive to a negative temperature gradient; our models currently allow only a single temperature gradient. To further investigate the atmospheric structure, we can invert the observed light curve, by assuming that the change in stellar flux is due entirely to a change in refractive properties of the atmosphere, which in turn is due to changing temperatures (Elliot et al. 2003b). In this way, we can retrieve the arbitrary temperature profile that is consistent with the observed light curves.

In Figure 7, we present the inversion of the HIPO-red light curve, both ingress and egress portions. We note that the ingress and egress are indistinguishable given the formal errors, indicating similar atmospheric structures at the ingress and egress points. Further, this inversion invalidates our previous atmospheric model: Pluto's atmosphere does not

exhibit a simple, constant temperature gradient. Instead, it displays a stratopause: a maximum of temperature at a radius of approximately 1200 km with a strong positive thermal gradient below, perhaps continuing down to the surface unless there is a troposphere (Stansberry et al. 1994) Above the temperature maximum is a weaker negative thermal gradient, approaching a temperature of 100 K at 1280 km where the inversion ends. A similar temperature structure has been found by others (Dias-Oliveira et al. 2015). The size of this final gradient, approximately 6 K/km, is consistent with the value of 6.4 ± 0.9 K/km found during the New Horizons radio occultation immersion data (Gladstone et al. 2016).

A startling consequence of this inversion is that the atmosphere appears to continue down to 1180 km (from the center of Pluto) before the inversion ends. Because Pluto's surface radius has been uncertain—no Earth-based occultation observation has ever reached Pluto's surface because refraction bends the light before then—all radii in the atmosphere traditionally have been quoted from the center of Pluto. Now, New Horizons imaging indicate that Pluto's surface radius is approximately 1187 km (Stern et al. 2015). Thus an atmosphere reading at 1180 km is non-physical; furthermore, the temperature at this radius is 100 K; if we use the derived lapse rate at 1180 km to extrapolate the temperature down to the expected surface temperature of 40 K, we find that this inversion predicts a surface radius of 1130 km.

The solution to this discrepancy lies in the fact that the occultation-light-curve inversion process assumes a clear atmosphere. All diminution of signal is interpreted as being due to refraction by the atmosphere. If instead the atmosphere contains a sufficient amount of haze this would mean that some of the signal loss is due to absorption/scattering rather than refraction. The result is that the entire temperature profile would move higher in the atmosphere. Thus, the combination of the inversion plus the New Horizons surface radius, given our multiwavelength observations, strongly implies that haze exists in Pluto's atmosphere, and particularly in the region probed by the occultation.

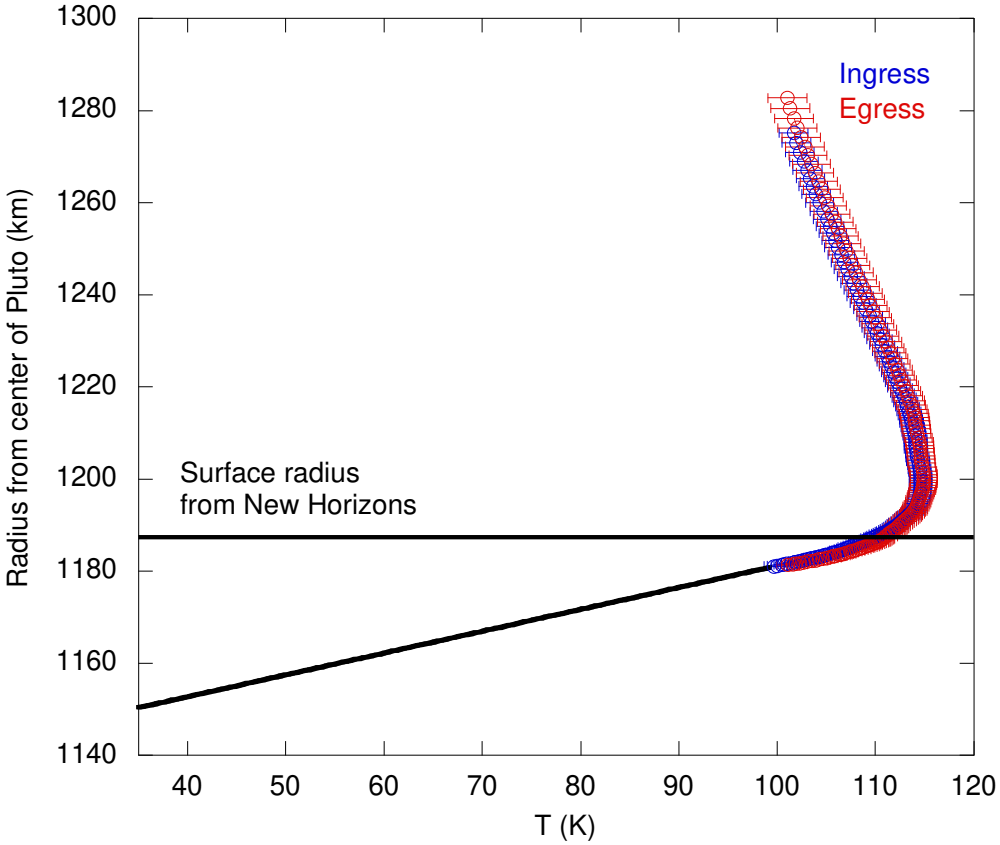

Fig. 7. Inversion of HIPO-red ingress and egress curves under the assumption of a clear atmosphere. The linear slope in the lower atmosphere is extended to the range of temperatures of the surface (40-50 K); the inversion thus predicts a surface radius of 1150 to 1160 km, in conflict with the New Horizons surface radius measurement of 1187 ± 4 km (Stern et al. 2015). Because this inversion extends below the surface radius value measured by New Horizons, this fact implies the presence of an absorber in Pluto's atmosphere, such as haze.

7 Discussion

For the optical and near-infrared data presented, a pure isothermal atmosphere model does not fit the data, nor does a continuous temperature gradient. Other possibilities include a hazy region in the atmosphere and/or a combination of thermal gradient(s) and isothermal layers. We show by the models presented in Table 4 and Fig. 6 that a thick, hazy region within the atmosphere produces an excellent fit to the data throughout the entire dataset, including around the central flash (which is sensitive to lower altitudes of the atmosphere). However, this does not rule out the possibility of a multi-region thermal gradient solution including a stratopause, as suggested by our inversion of the data. A clear atmosphere solution with appropriately placed thermal gradients, such as that postulated by Sicardy et al. (2016), is a viable fit to any individual light curve as well.

One way to discriminate between these various possibilities is to investigate the dependence of the light-curve parameters on wavelength (see Elliot et al. 2003 for previous work along these lines). We show in Fig. 8 the similarities and differences

among the HIPO-blue, HIPO-red, FPI+, and FLITECAM data, all taken simultaneously from SOFIA. The minimum flux is the flux level at the bottom of the light curve. This flux level has never reached 0 for any Pluto occultation yet observed, meaning that a small amount of residual starlight is always visible, even at the deepest portions of the occultations. This holds for the occultations in which central flash structures are seen as well. The most immediate implication of this is that no Pluto occultation has yet extended down far enough in the atmosphere to reach the surface; this is a result of the refractive properties of the atmospheres, not of the event geometry. In fact, this residual flux is expected for all observations except for those at very long wavelengths such as the REX occultation measurements at radio wavelengths, observed aboard the New Horizons spacecraft (Hinson et al. 2015); such radio-occultation measurements are not possible from Earth.

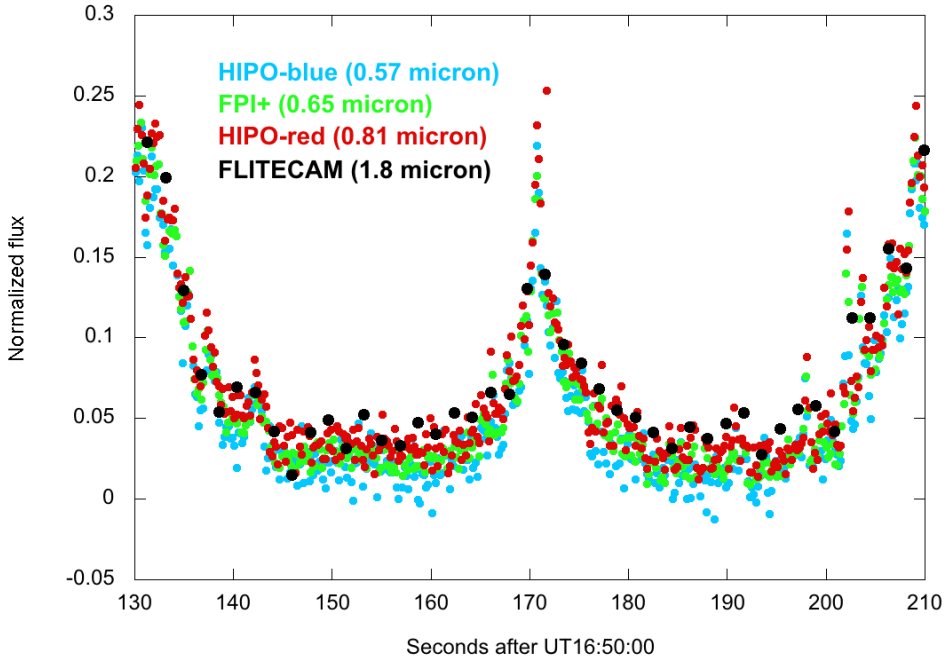

Fig. 8. Light curve lower baseline at multiple wavelengths, each taken contemporaneously from SOFIA. The minimum flux at the bottom of the light curves reaches different levels for the different observational wavelengths. The effective central wavelength for each observation is: 0.57 microns for HIPO-blue (in blue), 0.65 microns for FPI+ (in green), 0.81 microns for HIPO-red (in red), and 1.8 microns for FLITECAM (in black).

The minimum flux value is critically dependent on the calibration of the ratio of fluxes from Pluto and the occulted star. Pluto is in a crowded field in the Milky Way (Fig. 9); when combined with the ~5 arcsec seeing aboard SOFIA, separated photometry is a difficult task. The SOFIA data are critical for this comparison; observations were collected simultaneously with three instruments, at four wavelengths. Given the SOFIA flight altitude of ~40,000 ft, the influence of atmospheric extinction was greatly reduced as well. Two data sets were obtained aboard SOFIA that can be used for these purposes: one during the test flight the night before, and one during the photometry leg of the occultation flight, approximately 5 hours before the occultation event. Each set of data

has its own challenges. The test flight data (previous night) represent a different Pluto phase, by 1/6 of its period. However, Pluto's pole position is such that this represents a small change of viewing area. The data set from the photometry leg (same night) has near-blended-image issues as Pluto and the occultation star are in close proximity, along with other background stars. After several trials, for SOFIA we chose to use data from the photometry leg (same night) with multiple-source PSF fitting to disentangle the contributions from Pluto+Charon and the occultation star. In these data, there is a background star that must be accounted for (visible as the fainter star on the right just outside the blue circle in Fig. 9); data from the previous night is used for this. The advantage of using the same-night data is important because flat-field frames were not able to be taken for any of the three instruments. A small amount of edge vignetting is visible in all datasets. By using same-night data, Pluto and the occultation star are close within the frame, and therefore flat-field correction is not necessary.

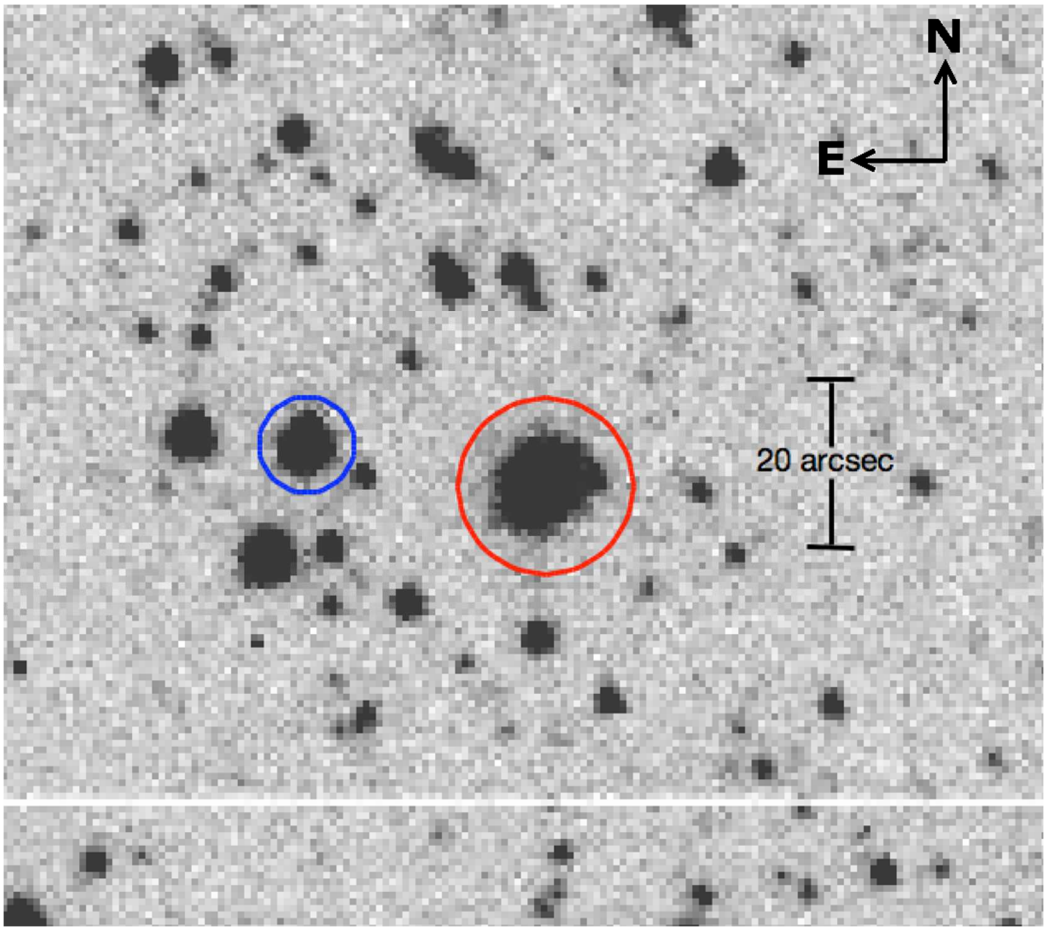

Fig. 9. A portion of a pre-event Pluto frame from SARA-CT, approximately 100 arcsec across, showing the crowded field near Pluto. The occultation star is circled in red; Pluto is circled in blue. This frame was taken approximately 7.5 hours before the occultation. The occultation was not visible from South America; this image was taken before teams in New Zealand and on SOFIA began observations for the event.

The residual stellar flux at the bottom of the light curve (Fig. 8), the minimum flux, is present because star light is strongly refracted by Pluto's atmosphere and thus stellar

signal is present, in small amounts, at mid-event. These stellar rays travel through the longest atmospheric path length and therefore are most susceptible to extinction by any atmospheric hazes, processes that will have a strong dependence on wavelength. This occultation event was designed such that the observations were obtained at multiple wavelengths, with central wavelengths from 0.57 to 1.8 microns. In particular, the HIPO/FLITECAM instrument combination aboard SOFIA, nicknamed FLIPO when used together, observes from the same beam from the telescope. While the observational parameters are different for each camera, these observations are contemporaneous and are observing the identical portion of Pluto's atmosphere. Note that while the central flash peak in Fig. 8 appears higher for HIPO-red, FPI+, and HIPO-blue than it does for FLITECAM, this is an artifact of the various observing parameters for the different instruments. Only FLITECAM has a deadtime between images (of 0.55 sec); FLITECAM's exposure time was 1.25 sec vs. 0.2 sec for HIPO-blue and HIPO-red. As a test, we simulated FLITECAM observing parameters by binning and skipping points (for the deadtime) from the HIPO-blue data stream; the HIPO-blue central flash peak then became equal to or lesser than the FLITECAM peak, depending on the phasing of the data chosen. Thus all data consistently maintain the wavelength ordering seen in Fig. 8: FLITECAM has the highest residual flux through the light curve bottom and central flash while HIPO-blue has the lowest residual flux in this same region.

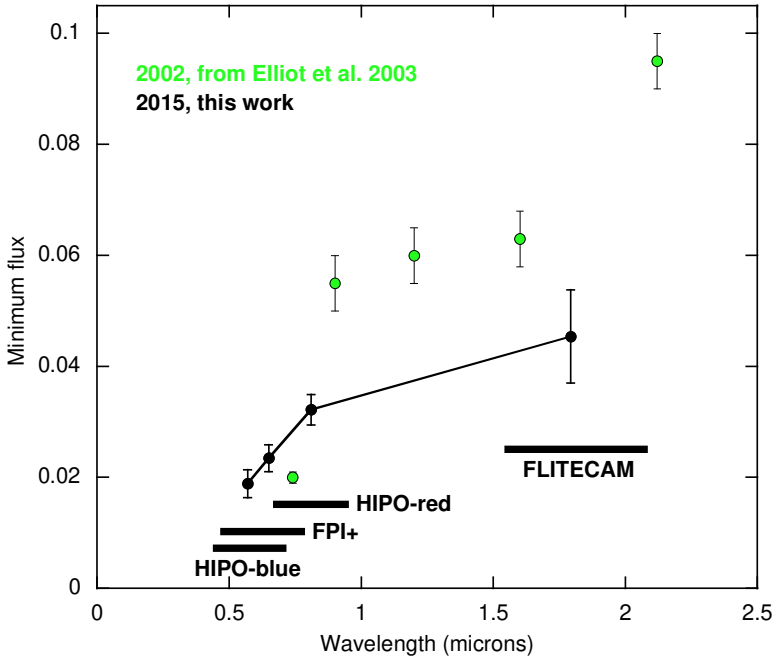

Fig. 10. Wavelength dependence of minimum flux value. If haze exists in the atmosphere (with small, sub-micron particles), we expect the minimum flux to be lowest for bluer wavelengths in this range. This trend is reflected by the minimum flux of the 2015 data. A similar trend was seen in the 2002 Pluto occultation (Elliot et al. 2003a); the 2002 data points are included in this plot in green for comparison.

If there were no hazes present in Pluto's atmosphere, we would expect little dependence of minimum flux on observational wavelength (Fig 10). Instead, the data in Fig. 10 show

a clear positive correlation between minimum flux and wavelength. While the overall light curve form could be reproduced by a clear atmospheric model in any single wavelength (see e.g., Sicardy et al. 2016), this flux dependence on wavelength can differentiate the two cases, and was one of the primary drivers for using the multi-chromatic capabilities of the SOFIA instruments. Indeed, this observation was one of the principal reasons the HIPO and FLITECAM teams worked so hard for so long to make the FLIPO configuration a reality

We model a haze that could cause the observed variation of flux with wavelength following Gulbis et al. (2015), which used rigorous Mie scattering theory and assumed dark, organic tholins. Tholins are selected because they have been detected on Pluto's surface (e.g., Grundy and Buie 2002; Olkin et al. 2007) and were used in the flux versus wavelength analysis for Pluto occultation data in 2002 (Elliot et al. 2003a). We consider the simple case, for spherical particles where the relative transmission of flux is determined by the combination of extinction along the line of sight and the atmospheric refraction: $T_{atm} * \exp(-\tau)$. We set $T_{atm}=0.05$, based on arguments in Elliot et al. (2003a) and Rannou and Durry (2009). Note that T_{atm} is half the value used in the analyses of the 2002 data, which is consistent with the 2015 minimum flux values being approximately half those observed in 2002 at similar wavelengths (Fig 10). The optical depth is given by

$$\tau = \begin{cases} n(a_0)\pi {a_0}^2 Q_{ext}, & \text{for single particle sizes} \\ \int_{a_{min}}^{a_{max}} n(a_0)\left(\frac{a_0}{a}\right)^q \pi a^2 Q_{ext} da\,, & \text{for a power law size distribution} \end{cases}, \qquad (1)$$

where a_0 is a reference particle radius, and a_{max} and a_{min} are the maximum and minimum particles sizes in a distribution. The column density is given by $n(a_0)$; this value is for the line-of-sight column and thus represents the value along a curved path for the minimum flux at the bottom of the light curve. The variable q represents the number density power, and the efficiency factor for extinction, Q_{ext}, is defined to be the sum of the efficiency factors for scattering and absorption (van de Hulst 1981). This power law form is a reasonable assumption given that it matches the size distribution for small atmospheric aerosols, impact ejecta, ring particles, and icy geysers on Enceladus (e.g. Welander 1959; Cours et al. 2011; Hartmann 1969; Shuvalov and Dypvik 2013; Marouf et al. 1983; Kempf et al. 2008; Schmidt et al. 2008). The extinction coefficient is highly dependent on the real and imaginary indices of refraction of the material. We begin by assuming the indices of refraction for tholins from Khare et al. (1984), interpolating between their listed data points.

Figure 11 shows the occultation flux data along with examples of modeled transmission for small, moderate, and large tholin haze particles. Submicron-sized particles return a positive correlation between flux and wavelength over the observed range, while multiple-micron-sized particles return a relatively flat line. The flux-versus-wavelength trends in the data are most like the 0.1 micron, single-particle size example. Assuming a reference particle radius halfway between minimum and maximum, the size-distribution model can be fit to the flux-versus-wavelength data with four parameters: a_{max}, a_{min}, q, and $n(a_0)$. The best-fit, least squares model is shown in Fig. 11 and has parameters listed

in Table 6. The model is highly dependent on particle sizes and number densities, yet depends only weakly on the power law of the particle size distribution.

The Khare et al. (1984) tholins were made from 0.9 N_2 and 0.1 CH_4, at a pressure of 0.2 mbar. Other laboratory measurements have been made for tholins having different compositions (e.g. 0.98 N_2 and 0.02 CH_4, 0.999 N_2 and 0.001 CH_4), at difference pressures (from 0.26 to 920 mbar), and using different measurement techniques (compilation in West et al. 2014). Tholin measurements have typically been produced in consideration of haze in Titan's atmosphere. While Pluto's atmosphere is thought to have a similar composition and scale height, the surface pressure (approximately 10 μbar) is a factor of ~10^5 lower and the solar flux is roughly 10% that of Titan and the charged particle environment is different in the Kuiper Belt than in the Saturn system (as discussed in Stansberry et al. 1989; Rannou and Durry 2009). Therefore, tholin properties are not well constrained for Pluto's atmosphere and more accurate models could be developed in the future.

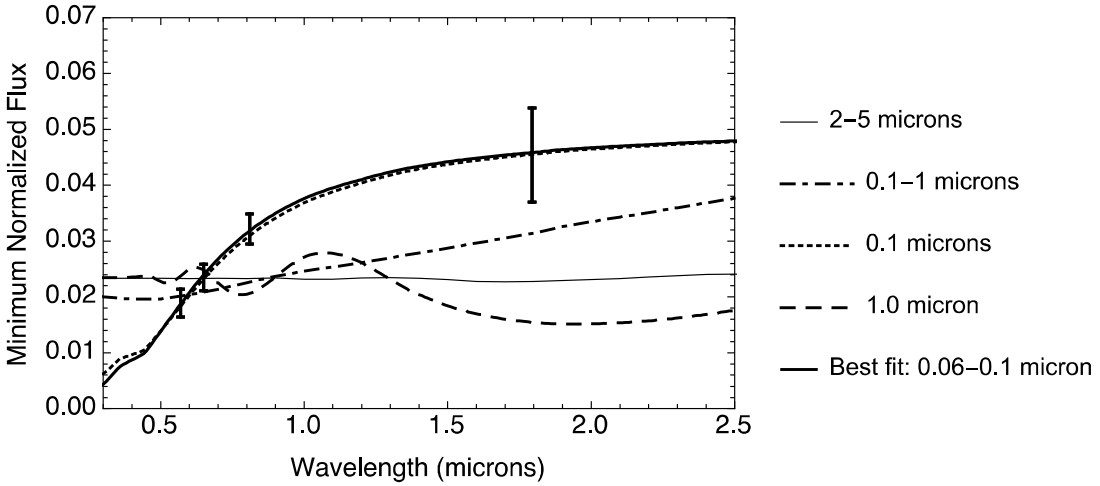

Figure 11. Minimum flux versus observed wavelength at the bottom of the lightcurve and examples of modeled transmission for a haze consisting of range of small particles (0.1–1 microns; dot-dash), small, single-sized particles (0.1 microns; dotted), moderate particles (1.0 microns; dashed), and a range of larger particles (2–5 microns; thin solid). The power law exponent q is 3.2, which is in line with that expected from fragmentation processes (e.g. Hartmann 1969). The best model fit to the data (0.06–0.1 microns; bold solid) is included, with parameters given in Table 6.

Table 6: Minimum flux best fit parameters for a particle size distribution

Quantity	Description	Value
a_{min}	Lower detectable limit on particle size distribution	0.060 ± 0.049 μm
a_{max}	Upper detectable limit on particle size distribution	0.100 ± 0.001 μm
a_0	Reference particle size	0.08 μm
$n(a_0)$	Line-of-sight column density	(1.687 ± 0.025) × 10^{11} cm^{-2}

q	Power law exponent	3.2 ± 5.4	
m	Complex index of refraction for tholins (Khare et al. 1984)	0.57 μm 0.65 μm 0.81 μm 1.8 μm	1.72 + 0.022i 1.68 + 0.016i 1.67 + 0.004i 1.64 + 0.0004i

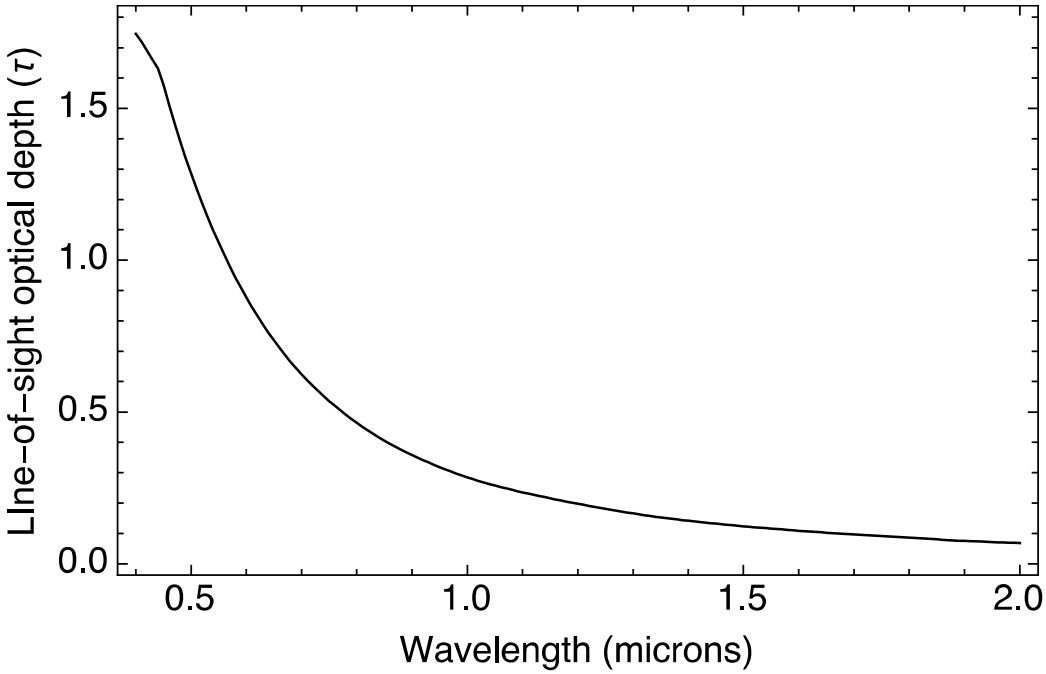

Figure 12. Line-of-sight optical depth as a function of observed wavelength, inferred from minimum flux measurements of the 29 June 2015 stellar occultation by Pluto. This plot was generated from Eq. (1), for the best-fit result parameters listed in Table 6. The optical depths increase sharply toward the blue end of the spectrum, indicative of prevalently small particle sizes. Passbands of the various camera filters are available in Figure 10 for comparison.

The variation of the minimum flux in Fig. 10, from 2% to 4% of the full star value, exhibits a dependence with wavelength. A Mie scattering model for spherical tholins demonstrates that this dependence can be caused by particles less than approximately 0.1 microns in radius. The corresponding optical depth for the best-fit model is shown in Fig. 12. A similar wavelength dependence was seen by Elliot et al. (2003a) using visible and near-IR occultation data from the UH 2.2m, IRTF, and CFHT (Fig. 10). They found that particles twice the size (~0.2 micron) of those found here had the appropriate wavelength dependence to match the 2002 Pluto occultation data. These results are thus consistent with previous findings and suggest that haze parameters can change over time.

We can compare our finding of haze particles in the 0.06 – 0.1-micron size range to evidence from New Horizons. Two primary pieces of evidence are available: the high phase angle image of Pluto surrounded by layered haze, taken at several wavelengths, and the absence of haze in low-phase angle images of Pluto. The New Horizons spacecraft captured a forward-scattering image of hazes in Pluto's atmosphere (Stern et

al. 2015; Gladstone et al. 2015) at a phase angle of 167˚. The spacecraft looked back at Pluto while the Sun was occulted; the entire perimeter of Pluto glowed a bright blue with haze structure visible around the limb. These observations were made with the panchromatic LORRI imager (Cheng et al. 2008) at 0.35 to 0.85 microns and with LEISA (Reuter et al. 2008). The LEISA data combined images taken at three wavelengths between 1.25 and 2.5 microns to produce a false-color image of the haze in the near infrared. Although exact values are not available at this time, this LEISA image shows a lower intensity for the haze than was visible in the LORRI image. The evidence from New Horizons is that the haze is brightest in their shortest wavelength images (0.35-0.85 microns), less bright at 1.25 microns, and even less bright at 2.5 microns. This dependence with wavelength is consistent with haze particles of order (or slightly smaller than) their shortest wavelength of observation, given the strongly forward-scattering nature of particles when observed at wavelengths similar to the particle sizes. The lack of haze detection at low phase angles (Cheng et al. 2015) is also consistent with ~0.1-micron particles, as the back-scattered intensity for these particles would be small. We take this as confirming evidence that the haze detected by New Horizons was also detected in our occultation data at lower altitudes.

The normal optical depth that was inferred from analysis of the New Horizons LORRI image of the haze was 0.004. In order to compare this to our analysis for particle optical depths (Fig. 12), we must first take into account the path length of the observation. For the stellar occultation, the residual stellar brightness at the bottom of the light curve results from star light that has been refracted through Pluto's atmosphere and around its limb, with light curves from SOFIA and Mt. John (Pasachoff et al. 2017) capturing the central flash. The stellar signal traverses approximately 25% of Pluto's circumference before being detected in the occultation signature. Correcting for this stark difference in path length, the observed τ_n corresponds to an increase in the line-of-sight τ by a factor of 30–60, rather than the more usual value of ~12 taken as $\sqrt{2\pi\,(r/H)}$ for the half-light altitude, making the τ_n =0.004 observed with New Horizons consistent with our observations of the haze. A different approach to calculating the line-of-sight optical depth for transiting exoplanets is given by Robinson et al. (2014) and Fortney (2005) with the result that the line-of-sight optical depth is enhanced over the normal optical depth by a factor of 35 to 90.

8 Conclusions

Observations of a stellar occultation by Pluto on 29 June 2015 show that the atmospheric pressure at half-light is consistent with that measured in 2013 (Bosh et al. 2015a) and 2011 (Person et al. 2013). Assuming the lower atmosphere temperature profile derived by New Horizons (Hinson et al. 2017) results in a derived surface pressure of 12.4 +/- 2.7 μbar (compare to Hinson *et al*. 2017 – 11.5 ± 0.7 μbar, and Sicardy *et al*. 2016 – 11.9–13.7 μbar). These various results (Linscott et al. 2015; Gladstone et al. 2015) (Hinson et al. 2017) indicate a general agreement among ground-based and New Horizons data and interpretations of atmospheric structure. As the 29 June 2015 event occurred just two weeks prior to the New Horizons encounter with Pluto, this event is an important

connection between decades of Earth-based observations and high-resolution, in situ measurements of Pluto's atmospheric and surface parameters.

The 29 June 2015 occultation was observed at several wavelengths simultaneously; the high SNR data obtained from instruments aboard SOFIA allowed us to investigate the wavelength dependence of the occultation light curves. Small differences in residual flux at the light curve minimum are evidence of small-particulate haze in Pluto's atmosphere. Based on the wavelength dependence of the minimum flux of occultation light curves, haze in Pluto's atmosphere was proposed by Elliot et al. (2003a) and Gulbis (2015). Due to the geometry of a stellar occultation, the path lengths through the atmosphere are long; this enhances the observed line-of-sight optical depth (Fig. 12). The magnitude of the minimum flux dependence on wavelength is very small; only those occultations with the highest SNR are able to see this effect. Additionally, analysis requires precise calibration of the relative photometry of Pluto/Charon and the occultation star, a task made more difficult by the crowded fields that Pluto currently traverses.

9 Acknowledgments

These critical observations with SOFIA would not have been possible if not for more than 30 years of tireless work and genius by the late Professor Dr. Hans-Peter Röser of the University of Stuttgart and by the late SOFIA Chief Engineer Mr. Nans Kunz of the NASA Ames Research Center.

The SOFIA portion of these observations would not have occurred without the scientific and management support of then SMO Deputy Director of Science William Reach and then SMO Director Erick Young. We also thank NASA SOFIA Program Manager Eddie Zavala and the entire SOFIA team for their support.

We thank Dick French, Georgi Mandushev, Tom Allen, Lauren Biddle, Lisa Prato, and Gail Schaefer for assistance during the prediction phase of this project.

JVC would like to thank Ken Bower—"for teaching me the general art of flight planning, and doing an amazing job absorbing the peculiarities of occultation flight planning in two long days before the check flight"; and Navigator Jeff "Elvis" Wilson for smoothly translating our needs into "pilot-speak" with a former bombardier's flair.

The FPI+ team thanks Karsten Schindler of DSI for his ground-based observations of the star field prior to the event, allowing accurate planning of the FPI+ settings.

This work is based, in part, on observations made with the NASA/DLR Stratospheric Observatory for Infrared Astronomy (SOFIA). SOFIA is jointly operated by the Universities Space Research Association, Inc. (USRA), under NASA contract NAS2-97001, and the Deutsches SOFIA Institut (DSI) under DLR contract 50 OK 0901 to the University of Stuttgart. Additional financial support for this work was provided by NASA through award #SOF 03-0028 issued by USRA.

Data were acquired using the Mt. John Observatory Optical Craftsman 61cm telescope, operated by the AAVSO and the University of Canterbury. We are grateful to Nigel Frost and Arne Henden for support at MJO, and to H. Roe for the loan of his near IR camera (Xeva-CL).

Some of the data presented herein were obtained at the W.M. Keck Observatory, which is operated as a scientific partnership among the California Institute of Technology, the University of California and the National Aeronautics and Space Administration. The Observatory was made possible by the generous financial support of the W.M. Keck Foundation.

This paper includes data gathered with the 6.5 meter Magellan Telescopes located at Las Campanas Observatory, Chile. Laird Close, Katie Morzinski, and Jared Males graciously helped with observations.

Support for this work was provided by NASA SSO grants NNX15AJ82G to Lowell Observatory, NNX10AB27G to MIT, and NNX12AJ29G to Williams College. AAS acknowledges support from the National Research Foundation of South Africa.

10 References

Bagenal, F., S. A. Stern, H. A. Weaver, L. A. Young, K. Ennico, C. Olkin, D. J. McComas, R. L. McNutt, M. Horanyi, H. A. Elliott, M. E. Hill, E. Zernstein, P. Kollman, S. M. Krimigis, C. M. Lisse, D. F. Strobel, J. Szalay, and M. Piquette 2015. Solar wind interaction with Pluto's escaping atmosphere. *Bulletin of the American Astronomical Society* **47**,

Becklin, E. E., A. G. G. M. Tielens, R. D. Gehrz, and H. H. S. Callis 2007. Stratospheric Observatory for Infrared Astronomy (SOFIA). *Society of Photo-Optical Instrumentation Engineers (SPIE) Conference* **6678**,

Bosh, A. S., M. J. Person, S. E. Levine, C. A. Zuluaga, A. M. Zangari, A. A. S. Gulbis, G. Schaefer, E. W. Dunham, B. A. Babcock, J. M. Pasachoff, P. Rojo, E. Servajean, F. Forster, T. Oswalt, D. Batcheldor, D. Bell, P. Bird, D. Fey, T. Fulwider, E. Geisert, D. Hastings, C. Keuhler, T. Mizusawa, P. Solenski, and B. Watson 2015a. The State of Pluto's Atmosphere in 2012-2013. *Icarus* **246**, 237-246.

Bosh, A. S., M. J. Person, C. A. Zuluaga, A. A. Sickafoose, S. E. Levine, J. M. Pasachoff, B. A. Babcock, E. W. Dunham, I. McLean, J. Wolf, F. Abe, E. Becklin, T. A. Bida, L. P. Bright, T. Brothers, G. Christie, P. L. Collins, R. F. Durst, A. C. Gilmore, R. Hamilton, H. C. Harris, C. Johnson, P. M. Kilmartin, M. R. Kosiarek, K. Leppik, S. E. Logsdon, R. Lucas, S. Mathers, C. J. K. Morley, P. Nelson, H. Ngan, E. Pfüller, T. Natusch, H.-P. Röser, S. Sallum, M. Savage, C. H. Seeger, H. Siu, C. Stockdale, D. Suzuki, T. Thanathibodee, T. Tilleman, P. J. Tristram, J. Van Cleve, C. Varughese, L. W. Weisenbach, E. Widen, and M. Wiedemann 2015b. Haze in Pluto's atmosphere: Results from SOFIA and ground-based observations of the 2015 June 29 Pluto occultation. *Bulletin of the American Astronomical Society* **47**,

Brown, A. G. A., A. Vallenari, T. Prusti, and H. J. de Bruijne 2018. GAIA Data Release 2. Summary of the contents and survey properties. *Astronomy & Astrophysics* **616**, 22.

Buie, M. W., W. M. Grundy, E. F. Young, L. A. Young, and S. A. Stern 2010. Pluto and Charon with the Hubble Space Telescope. II. Resolving changes on Pluto's surface and a map for Charon. *Astronomical Journal* **139**, 1128-1143.

Cheng, A. F., R. Gladstone, M. Summers, A. Parker, J. Spencer, L. Young, H. Weaver, K. Ennico, C. Olkin, and A. Stern 2015. Discovery of hazes in Pluto's atmosphere. *Bulletin of the American Astronomical Society* **47**,

Cheng, A. F., H. A. Weaver, S. J. Conard, M. F. Morgan, O. Barnouin-Jha, J. D. Boldt, K. A. Cooper, E. H. Darlington, M. P. Grey, J. R. Hayes, K. E. Kosakowski, T. Magee, E. Rossano, D. Sampath, C. Schlemm, and H. W. Taylor 2008. Long-Range Reconnaissance Imager on New Horizons. *Space Science Reviews* **140**, 189-215.

Close, L. M., V. Gasho, D. Kopon, J. Males, K. B. Follette, K. Brutlag, A. Uomoto, and T. Hare 2010. The Magellan Telescope adaptive secondary AO system: a visible and mid-IR AO facility. *Proceedings of the SPIE* **7736**, 773605.

Cours, T., J. Burgalat, P. Rannou, S. Rodriguez, A. Brahic, and R. A. West 2011. Dual Origin of Aerosols in Titan's Detached Haze Layer. *Astrophysical Journal Letters* **741**, 5.

Dias-Oliveira, A., B. Sicardy, E. Lellouch, R. Vieira-Martins, M. Assafin, J. I. B. Camargo, F. Braga-Ribas, A. R. Gomes-Júnior, G. Benedetti-Rossi, F. Colas, A. Decock, A. Doressoundiram, C. Dumas, M. Emilio, J. Fabrega Polleri, R. Gil-Hutton, M. Gillon, J. H. Girard, G. K. T. Hau, V. D. Ivanov, E. Jehin, J. Lecacheaux, R. Leiva, C. Lopez-Sisterna, L. Mancini, J. Manfroid, A. Maury, E. Meza, N. Morales, L. Nagy, C. Opitom, J. L. Ortiz, J. Pollock, F. Roques, C. Snodgrass, J. F. Soulier, A. Thirouin, L. Vanzi, T. Widemann, D. E. Reichart, A. P. Lacluyze, J. B. Haislip, K. M. Ivarsen, M. Dominik, U. G. Jørgensen, and J. Skottfelt 2015. Pluto's atmosphere from stellar occultations in 2012 and 2013. *Astrophysical Journal* **811**,

Dunham, E. W., J. L. Elliot, T. A. Bida, and B. W. Taylor 2004. HIPO: A high-speed imaging photometer for occultations. *Society of Photo-Optical Instrumentation Engineers (SPIE) Conference* **5492**, 592-603.

Elliot, J. L., A. Ates, B. A. Babcock, A. S. Bosh, M. W. Buie, K. B. Clancy, E. W. Dunham, S. S. Eikenberry, D. T. Hall, S. D. Kern, S. K. Leggett, S. E. Levine, D.-S. Moon, C. B. Olkin, D. J. Osip, J. M. Pasachoff, B. E. Penprase, M. J. Person, S. Qu, J. T. Rayner, L. C. Roberts Jr., C. V. Salyk, S. P. Souza, R. C. Stone, B. W. Taylor, D. J. Tholen, J. E. Thomas-Osip, D. R. Ticehurst, and L. H. Wasserman 2003a. The recent expansion of Pluto's atmosphere. *Nature* **424**, 165-168.

Elliot, J. L., M. J. Person, and S. Qu 2003b. Analysis of stellar occultation data. II. Inversion, with application to Pluto and Triton. *Astronomical Journal* **126**, 1041-1079.

Fortney, J. J. 2005. The effect of condensates on the characterization of transiting planet atmospheres with transmission spectroscopy. *Monthly Notices of the Royal Astronomical Society* **364**, 649-653.

Gladstone, G. R., A. Stern, K. Ennico, C. Olkin, H. A. Weaver, L. A. Young, M. E. Siummers, D. Strobel, D. P. Hinson, J. Kammer, A. Parker, A. Steffl, I. Linscott, J. Parker, A. F. Cheng, D. C. Slater, M. Versteeg, T. Greathouse, K. Retherford, H. Throop, N. Cunningham, W. Woods, K. Singer, C. Tsang, E. Schindhelm, C. M. Lisse, M. L. Wong, Y. L. Yung, X. Zhu, W. Curdt, P. Lavvas, E. Young, and G. L. Tyler 2016. The atmosphere of Pluto as observed by New Horizons. *Science* **351**,

Gladstone, G. R., S. A. Stern, H. A. Weaver, L. A. Young, K. A. Ennico, C. B. Olkin, A. F. Cheng, T. K. Greathouse, D. P. Hinson, J. A. Kammer, I. R. Linscott, A. H. Parker, J. W. Parker, K. D. Retherford, E. Schindhelm, K. N. Singer, A. J. Steffl, D. F. Strobel, M. E. Summers, C. C. C. Tsang, G. L. Tyler, M. H. Versteeg, W. W. Woods, N. Cunningham, and W. Curdt 2015. New Horizons observations of the atmospheres of Pluto and Charon. *Bulletin of the American Astronomical Society* **47**, 100.05.

Grundy, W. M., and M. W. Buie 2002. Spatial and Compositional Constraints on Non-ice components and H20 on Pluto's Surface. *Icarus* **157**, 128-138.

Gulbis, A. A. S., J. P. Emery, M. J. Person, A. S. Bosh, C. A. Zuluaga, J. M. Pasachoff, and B. A. Babcock 2015. Observations of a successive stellar occultation by Charon and graze by Pluto in 2011. *Icarus* **246**, 226-236.

Hansen, C. J., and D. A. Paige 1996. Seasonal nitrogen cycles on Pluto. *Icarus* **120**, 247-265.

Hansen, C. J., D. A. Paige, and L. A. Young 2015. Pluto's climate modeled with new observational constraints. *Icarus* **246**, 183-191.

Hartmann, W. K. 1969. Terrestrial, lunar, and interplanetary rock fragmentation. *Icarus* **10**, 201-213.

Henden, A., and U. Munari 2014. The APASS all-sky, multi-epoch BVgri photometric survey. *Contributions of the Astronomical Observatory Skalnaté Pleso* **43**, 518-522.

Henden, A. A., S. Levine, D. Terrell, and D. L. Welch 2015. APASS - the latest data release. *Bulletin of the American Astronomical Society* **225**,

Hinson, D. P., I. Linscott, L. Tyler, M. Bird, M. Paetzold, D. Strobel, M. Summers, W. Woods, A. Stern, H. Weaver, C. Olkin, L. Young, K. Ennico, R. Gladstone, T. Greathouse, J. Kammer, A. Parker, J. Parker, K. Retherford, E. Schindhelm, K. Singer, A. Steffl, C. Tsang, and M. Versteeg 2015. Radio occultation measurements of Pluto's atmosphere with New Horizons. *Bulletin of the American Astronomical Society* **47**, 105.01.

Hinson, D. P., I. R. Linscott, L. A. Young, G. L. Tyler, S. A. Stern, R. A. Beyer, M. K. Bird, K. Ennico, G. R. Gladstone, C. B. Olkin, M. Pätzold, P. M. Schenk, D. F. Strobel, M. E. Summers, H. A. Weaver, and W. W. Woods 2017. Radio occultation measurements of Pluto's neutral atmosphere with New Horizons. *Icarus* **290**, 96-111.

Kempf, S., U. Beckmann, G. Morgas-Klostermeyer, F. Postberg, R. Srama, T. Economou, J. Schmidt, F. Spahn, and E. Grun 2008. The E ring in the vicinity of Enceladus. I. Spatial distribution and properties of the ring particles. *Icarus* **193**, 420-437.

Khare, B. N., C. Sagan, E. T. Arakawa, F. Suits, T. A. Callcott, and M. W. Williams 1984. Optical constants of organic tholins produced in a simulated Titanian atmosphere: From soft X-ray to microwave frequencies. *Icarus* **60**, 127-137.

Lellouch, E., B. Sicardy, C. de Bergh, H.-U. Käufl, S. Kassi, and A. Campargue 2009. Pluto's lower atmosphere structure and methane abundance from high-resolution spectroscopy and stellar occultations. *Astronomy and Astophysics* **495**, L17-L21.

Linscott, I. R., A. Stern, H. Weaver, L. Young, C. Olkin, and K. A. Ennico 2015. First results from the New Horizons Radio Science experiment: Measurements of Pluto's atmospheric structure, surface pressure, and microwave brightness temperature. *Bulletin of the American Astronomical Society* **47**, 101.03.

Lockhart, M., M. J. Person, J. L. Elliot, and S. P. Souza 2010. PICO: Portable Instrument for Capturing Occultations. *Publications of the Astronomical Society of the Pacific* **122**, 1207-1213.

Logsdon, S. E., I. S. McLean, E. E. Becklin, E. W. Dunham, R. T. Hamilton, C. Johnson, J. W. Milburn, M. L. Savage, S. S. Shenoy, E. C. Smith, and W. D. Vacca 2014. FLITECAM: early commissioning results. *Society of Photo-Optical Instrumentation Engineers (SPIE) Conference* **9147**,

Marouf, E. A., G. L. Tyler, H. A. Zebker, R. A. Simpson, and V. R. Eshleman 1983. Particle size distributions in Saturn's rings from Voyager 1 radio occultation. *Icarus* **54**, 189-211.

McLean, I. S., E. C. Smith, T. Aliado, G. Brims, E. Kress, E. Magnone, J. Milburn, A. Oldag, T. Silvers, G. Skulason, E. E. Becklin, and R. Y. Shiuping 2006. FLITECAM: A 1-5 micron camera and spectrometer for SOFIA. *Society of Photo-Optical Instrumentation Engineers (SPIE) Conference* **6269**, 168.

McNutt, R. L., M. E. Hill, C. M. Lisse, P. Kollmann, F. Bagenal, S. M. Krimigis, D. J. McComas, H. A. Elliott, S. J. Wolk, D. F. Strobel, X. Zhu, S. A. Stern, H. A. Weaver, L. A. Young, K. Ennico, and C. B. Olkin 2015. Escape of Pluto's Atmosphere: In Situ Measurements from the Pluto Energetic Particle Spectrometer Science Investigation (PEPSSI) instrument on New Horizons and Remote Observations from the Chandra X-ray observatory. *Bulletin of the American Astronomical Society* **47**,

Olkin, C. B., E. F. Young, W. Grundy, B. Schmitt, A. Tokunaga, T. Owen, T. Roush, and H. Terada 2007. Pluto's spectrum from 1.0 to 4.2 μm: Implications for surface properties. *Astronomical Journal* **133**, 420-431.

Olkin, C. B., L. A. Young, D. Borncamp, A. Pickles, B. Sicardy, M. Assafin, F. B. Bianco, M. W. Buie, A. D. de Oliveira, M. Gillon, R. G. French, A. Ramos Gomes, E. Jehin, N. Morales, C. Opitom, J. L. Ortiz, A. Maury, M. Norbury, F. Braga-Ribas, R. Smith, L. H. Wasserman, E. F. Young, M. Zacharias, and N. Zacharias 2015. Evidence that Pluto's atmosphere does not collapse from occultations including the 2013 May 04 event. *Icarus* **246**, 220-225.

Olkin, C. B., L. A. Young, R. G. French, E. F. Young, M. W. Buie, R. R. Howell, J. Regester, C. R. Ruhland, T. Natusch, and D. J. Ramm 2014. Pluto's atmospheric structure from the July 2007 stellar occultation. *Icarus* **239**, 15-22.

Pasachoff, J. M., B. A. Babcock, R. F. Durst, C. H. Seeger, S. E. Levine, A. S. Bosh, M. J. Person, A. A. Sickafoose, C. A. Zuluaga, M. R. Kosiarek, F. Abe, M. Nagakane, D. Suzuki, P. J. Tristram, and A. Arredondo 2017. Pluto occultation on

2015 June 29 UTC with central flash and atmospheric spikes just before the New Horizons flyby. *Icarus* **296**, 305-314.

Pasachoff, J. M., B. A. Babcock, R. F. Durst, C. H. Seeger, S. E. Levine, A. S. Bosh, A. A. Sickafoose, M. J. Person, F. Abe, D. Suzuki, M. Nagakane, and P. J. Tristam 2015. A Central Flash at an Occultation of a Bright Star by Pluto Soon Before New Horizons' Flyby. *Bulletin of the American Astronomical Society* **47**,

Perryman, M. A. C. 2002. GAIA: An Astrometric and Photometric Survey of our Galaxy. *Astrophysics and Space Science* **280**, 1-10.

Person, M. J., A. S. Bosh, S. E. Levine, A. A. S. Gulbis, A. M. Zangari, C. A. Zuluaga, J. M. Pasachoff, B. A. Babcock, S. Pandey, D. Amrhein, S. Sallum, E. W. Dunham, D. J. Tholen, P. Collins, T. Bida, B. Taylor, J. Wolf, A. Meyer, E. Pfueller, M. Wiedemann, H.-P. Roeser, R. Lucas, M. Kakkala, J. Ciotti, S. Plunkett, N. Hiraoka, W. Best, E. J. Pilger, M. Miceli, A. Springmann, M. Hicks, B. Thackeray, J. Emery, S. Rapoport, I. Ritchie, M. Pearson, A. Matingly, J. Brimacombe, D. Gault, R. Jones, R. Nolthenius, J. Broughton, and T. Barry 2013. The 2011 June 23 Stellar Occultation by Pluto: Airborne and Ground Observations. *Astronomical Journal* **146**, 15.

Person, M. J., A. S. Bosh, A. A. Sickafoose, C. A. Zuluaga, S. E. Levine, J. M. Pasachoff, B. A. Babcock, E. W. Dunham, I. McLean, J. Wolf, F. Abe, E. Becklin, T. A. Bida, L. P. Bright, T. C. Brothers, G. Christie, P. L. Collins, R. F. Durst, A. C. Gilmore, R. Hamilton, H. C. Harris, C. Johnson, P. M. Kilmartin, M. R. Kosiarek, K. Leppik, S. E. Logsdon, R. Lucas, S. Mathers, C. J. K. Morley, T. Natusch, P. Nelson, H. Ngan, E. Pfueller, H.-P. Roeser, S. Sallum, M. Savage, C. H. Seeger, H. Siu, C. Stockdale, D. Suzuki, T. Thanathibodee, T. Tilleman, P. J. Tristram, J. Van Cleeve, C. Varughese, L. W. Weisenbach, E. Widen, and M. Wiedemann 2015. Central Flash Analysis of the 29 June 2015 Occultation. *Bulletin of the American Astronomical Society* **47**,

Pfueller, E., J. Wolf, and M. Wiedemann 2018. The SOFIA Focal Plane Imager: A Highly Sensitive and Fast Photometer for the Wavelength Range 0.4 to 1 Micron. *Journal of Astronomical Instrumentation* **07**,

Rannou, P., and G. Durry 2009. Extinction layer detected by the 2003 star occultation on Pluto. *Journal of Geophysical Research* **114**,

Reuter, D. C., S. A. Stern, J. Scherrer, D. E. Jennings, J. W. Baer, J. Hanley, L. Hardaway, A. Lunsford, S. McMuldroch, J. Moore, C. Olkin, R. Parizek, H. Reitsema, D. Sabatke, J. Spencer, J. Stone, H. Throop, J. van Cleve, G. E. Weigle, and L. A. Young 2008. Ralph: A visible/infrared imager for the New Horizons Pluto/Kuiper Belt Mission. *Space Science Reviews* **140**, 129-154.

Robinson, T. D., L. Maltagliati, M. S. Marley, and J. J. Fortney 2014. Titan solar occultation observations reveal transit spectra of a hazy world. *Proceedings of the National Academy of Sciences* **111**, 9042-9047.

Schmidt, J., N. Brilliantov, F. Spahn, and S. Kempf 2008. Slow dust in Enceladus' plume from condensation and wall collisions in tiger stripe fractures. *Nature* **451**, 685-688.

Shuvalov, V., and H. Dypvik 2013. Distribution of ejecta from small impact craters. *Metoritics & Planetary Science* **48**, 1034-1042.

Sicardy, B., F. Colas, T. Widemann, A. Bellucci, W. Beisker, M. Kretlow, F. Ferri, S. Lacour, J. Lecacheux, E. Lellouch, S. Pau, S. Renner, F. Roques, A. Fienga, C. Etienne, C. Martinez, I. S. Glass, D. Baba, T. Nagayama, T. Nagata, S. Itting-Enke, K.-L. Bath, H.-J. Bode, F. Bode, H. Lu¨demann, J. Lu¨demann, D. Neubauer, A. Tegtmeier, C. Tegtmeier, B. Thome´, F. Hund, C. deWitt, B. Fraser, A. Jansen, T. Jones, P. Schoenau, C. Turk, P. Meintjies, M. Hernandez, D. Fiel, E. Frappa, A. Peyrot, J. P. Teng, M. Vignand, G. Hesler, T. Payet, R. R. Howell, M. Kidger, J. L. Ortiz, O. Naranjo, P. Rosenzweig, and M. Rapaport 2006. The two Titan stellar occultations of 14 November 2003. *Journal of Geophysical Research* **111**, E11S91-E11S116.

Sicardy, B., J. Talbot, E. Meza, J. Camargo, J. Desmars, D. Gault, D. Herald, S. Kerr, H. Pavlov, F. Braga-Ribas, M. Assafin, G. Benedetti-Rossi, A. Dias-Oliveira, A. R. Gomes-Júnior, R. Vieira Martins, D. Berard, P. Kervella, J. Lecacheaux, E. Lelloch, W. Beisker, D. Dunham, M. Jelinek, R. Duffard, J. Ortiz, A. J. Castro-Tirado, R. Cunniffe, R. Querel, P. C. Yock, A. A. Cole, A. B. Giles, K. M. Hill, J. P. Beaulieu, M. Harnisch, R. Jansen, A. Pennell, S. Todd, W. H. Allen, P. B. Graham, B. Loader, G. McKay, J. Milner, S. Parker, M. A. Barry, J. Bradshaw, J. Broughton, L. Davis, H. Devillepoix, J. Drummond, L. Field, M. Forbes, D. Giles, R. Glassey, R. Groom, D. Hooper, R. Horvat, G. Hudson, R. Idaczyk, D. Jenke, B. Lade, J. Newman, P. Nosworthy, P. Purcell, P. F. Skilton, M. Streamer, M. Unwin, H. Watanabe, G. L. White, and D. Watson 2016. Pluto's atmosphere from the 2015 June 29 ground-based stellar occultation at the time of the New Horizons flyby. *Astrophysical Journal Letters* **819**, L38.

Sickafoose, A. A., A. S. Bosh, M. J. Person, C. A. Zuluaga, S. E. Levine, J. M. Pasachoff, B. A. Babcock, E. W. Dunham, I. McLean, J. Wolf, F. Abe, T. A. Bida, L. P. Bright, T. Brothers, G. Christie, P. L. Collins, R. F. Durst, A. C. Gilmore, R. Hamilton, H. C. Harris, C. Johnson, P. M. Kilmartin, M. R. Kosiarek, K. Leppik, S. Logsdon, R. Lucas, S. Mathers, C. J. K. Morley, T. Natusch, P. Nelson, H. Ngan, E. Pfüller, H.-P. Roeser, S. Sallum, M. Savage, C. H. Seeger, H. Siu, C. Stockdale, D. Suzuki, T. Thanathibodee, T. Tilleman, P. J. Tristam, J. Van Cleve, C. Varughese, L. W. Weisenbach, E. Widen, and M. Wiedemann 2015. Investigation of particle sizes in Pluto's atmosphere from the 29 June 2015 occultation. *Bulletin of the American Astronomical Society* **47**,

Skrutskie, M. F., R. M. Cutri, R. Stiening, M. D. Weinberg, S. Schneider, J. M. Carpenter, C. Beichman, R. Capps, T. Chester, J. Elias, J. Huchra, J. Liebert, C. Lonsdale, D. G. Monet, S. Price, P. Seitzer, T. Jarrett, J. D. Kirkpatrick, J. E. Gizis, E. Howard, T. Evans, J. Fowler, L. Fullmer, R. Hurt, R. Light, E. L. Kopan, K. A. Marsh, H. L. McCallon, R. Tam, S. Van Dyk, and S. Wheelock 2006. The Two Micron All Sky Survey (2MASS). *Astronomical Journal* **131**, 1163-1183.

Souza, S. P., B. A. Babcock, J. M. Pasachoff, A. A. S. Gulbis, J. L. Elliot, M. J. Person, and J. W. Gangestad 2006. POETS: Portable Occultation, Eclipse, and Transit System. *Publications of the Astronomical Society of the Pacific* **118**, 1550-1557.

Stansberry, J. A., J. I. Lunine, W. B. Hubbard, R. V. Yelle, and D. M. Hunten 1994. Mirages and the nature of Pluto's atmosphere. *Icarus* **111**, 503-513.

Stansberry, J. A., J. I. Lunine, and M. G. Tomasko 1989. Upper limits on possible photochemical hazes on Pluto. *Geophysical Research Letters* **16**, 1221-1224.

Stern, S. A., F. Bagenal, K. Ennico, G. R. Gladstone, W. M. Grundy, W. B. McKinnon, J. M. Moore, C. B. Olkin, J. R. Spencer, H. A. Weaver, L. A. Young, T. Andert, J. Andrews, M. Banks, B. Bauer, J. Bauman, O. S. Barnouin, P. Bedini, K. Beisser, R. A. Beyer, S. Bhaskaran, R. P. Binzel, E. Birath, M. Bird, D. J. Bogan, A. Bowman, V. J. Bray, M. Brozovic, C. Bryan, M. R. Buckley, M. W. Buie, B. J. Buratti, S. S. Bushman, A. Calloway, B. Carcich, A. F. Cheng, S. Conard, C. A. Conrad, J. C. Cook, D. P. Cruikshank, O. S. Custodio, C. M. Dalle Ore, C. Deboy, Z. J. B. Dischner, P. Dumont, A. M. Earle, H. A. Elliott, J. Ercol, C. M. Ernst, T. Finley, S. H. Flanigan, G. Fountain, M. J. Freeze, T. Greathouse, J. L. Green, Y. Guo, M. Hahn, D. P. Hamilton, S. A. Hamilton, J. Hanley, A. Harch, H. M. Hart, C. B. Hersman, A. Hill, M. E. Hill, D. P. Hinson, M. E. Holdridge, M. Horanyi, A. D. Howard, C. J. A. Howett, C. Jackman, R. A. Jacobson, D. E. Jennings, J. A. Kammer, H. K. Kang, D. E. Kaufmann, P. Kollmann, S. M. Krimigis, D. Kusnierkiewicz, T. R. Lauer, J. E. Lee, K. L. Lindstrom, I. R. Linscott, C. M. Lisse, A. W. Lunsford, V. A. Mallder, N. Martin, D. J. McComas, R. L. McNutt, D. Mehoke, T. Mehoke, E. D. Melin, M. Mutchler, D. Nelson, F. Nimmo, J. I. Nunez, A. Ocampo, W. M. Owen, M. Paetzold, B. Page *et al.* 2015. The Pluto system: initial results from its exploration by New Horizons. *Science* **350**,

Strobel, D. F., X. Zhu, M. E. Summers, and M. H. Stevens 1996. On the vertical thermal structure of Pluto's atmosphere. *Icarus* **120**, 266-289.

van de Hulst, H. C. 1981. *Light Scattering by Small Particles.* Dover, New York.

Welander, P. 1959. A theoretical power-law for the size distribution of small particles or drops falling through the atmosphere. *Tellus* **11**, 197-201.

West, R., P. Lavvas, C. Anderson, and H. Imanaka 2014. Titan's haze. In *Titan: Interior, Surface, Atmosphere, and Space Environment* (I. C. F. Müller-Wodarg, C. A. Griffith, E. Lellouch and T. E. Cravens, Ed.), pp. 285-321. Cambridge University Press, Cambridge, UK.

Wolf, J., M. Wiedemann, E. Pfuller, M. Lachenmann, H. J. Hall, and H.-P. Roser 2014. *Upgrade of the SOFIA target acquisition and tracking cameras*. pp 11.

Yelle, R. V., and J. I. Lunine 1989. Evidence for a molecule heavier than methane in the atmosphere of Pluto. *Nature* **339**, 288-290.

Young, L., B. Sicardy, T. Widemann, M. J. Brucker, M. W. Buie, B. Fraser, H. Van Heerden, R. R. Howell, K. Lonergan, C. B. Olkin, H. J. Reitsema, A. Richter, T. Sepersky, L. H. Wasserman, and E. F. Young 2010. Results from the 2010 Feb 14 and July 4 Pluto occultations. *Bulletin of the American Astronomical Society* **42**, 982.

Young, L. A. 2013. Pluto's Seasons: New Predicitons for New Horizons. *Astrophysical Journal Letters* **766**, L22-L28.

Zacharias, N., S. E. Urban, M. I. Zacharias, G. L. Wycoff, D. M. Hall, D. G. Monet, and T. J. Rafferty 2004. The second US Naval Observatory CCD Astrograph Catalog (UCAC2). *Astronomical Journal* **127**, 3043-3059.

Zalucha, A. M., X. Zhu, A. A. S. Gulbis, D. F. Strobel, and J. L. Elliot 2011. An investigation of Pluto's troposphere using stellar occultation light curves and an atmospheric radiative-conductive-convective model. *Icarus* **214**, 685-700.